isvr Institute of Sound and Vibration Research

Ground-borne Vibration and Noise from Trains: Elastodynamic Analysis using the Combined Boundary Element and Finite Element Methods

C.J.C. Jones, D.J. Thompson and M. Petyt

ISVR Technical Memorandum 844

October 1999

University of Southampton

SCIENTIFIC PUBLICATIONS BY THE ISVR

Technical Reports are published to promote timely dissemination of research results by ISVR personnel. This medium permits more detailed presentation than is usually acceptable for scientific journals. Responsibility for both the content and any opinions expressed rests entirely with the author(s).

Technical Memoranda are produced to enable the early or preliminary release of information by ISVR personnel where such release is deemed to the appropriate. Information contained in these memoranda may be incomplete, or form part of a continuing programme; this should be borne in mind when using or quoting from these documents.

Contract Reports are produced to record the results of scientific work carried out for sponsors, under contract. The ISVR treats these reports as confidential to sponsors and does not make them available for general circulation. Individual sponsors may, however, authorize subsequent release of the material.

UNIVERSITY OF SOUTHAMPTON

INSTITUTE OF SOUND AND VIBRATION RESEARCH

DYNAMICS GROUP

Ground-borne Vibration and Noise from Trains: Elastodynamic Analysis using the Combined Boundary Element and Finite Element Methods

by

C.J.C. Jones, D.J. Thompson and M. Petyt

ISVR Technical Memorandum No. 844

October 1999

Authorized for issue by
Dr. M.J. Brennan
Group Chairman

SUMMARY

Previous work has demonstrated that a boundary element model with three-noded elements, having quadratic shape function interpolation, is successful in modelling ground vibration propagation in two dimensions up to 200 Hz. Here the method is extended to allow multiple boundary element domains to be linked together with structures modelled using finite elements. This forms a versatile model for studying the propagation of ground vibration from trains.

This report describes the theoretical background to a model that is implemented in the software package 'TEA'. Instructions for the use of the software and example results investigating the accuracy of the model are covered in a separate report.

For the boundary element domains special provision for open boundaries has been made so that the infinite ground surface or infinite interfaces between ground layers can be modelled as open boundaries of finite length. This approach has already been established in earlier work on single boundary element domains. The boundary element matrices are used to construct a dynamic stiffness matrix in terms of nodal forces. Finite element mass, stiffness and damping matrices are produced by the standard finite element method. These are then assembled with the BE dynamic stiffness matrices to form a global system of equations that can be solved for the complex amplitudes of displacement in response to applied nodal forces.

The usefulness of the method is demonstrated by the example analysis of the transmission of vibration from a bored tunnel and a cut-and-cover tunnel. The bored tunnel is 20 m below the ground surface (at rail height) and the results for a tunnel with and without a concrete lining are compared. For the cut-and-cover tunnel, the effect of stiffening the foundation to the abutment walls with short piles is demonstrated.

CONTENTS

GLOSSARY OF SYMBOLS

Δ	Dilatation
∇^2	Laplacian operator
δ_{lk}	Kroneker delta
$\delta\mathbf{u}$	Vector of applied virtual displacements
δu^j	Vector of applied virtual nodal displacements on element j
δw	Virtual work due to $\delta\mathbf{u}$
ε^i	2×2 tensor of principal value terms at the singular integration point i on the boundary
ε_x, ε_y	Principal components of strain
γ_{xy}	Shear strain component
η	Loss factor
λ, μ	Lamé constants
Γ	Boundary of domain for BE formulation
ν	Poisson's ratio
ξ	Non-dimensional internal co-ordinate defining any point within the element
ϕ_i	Shape function relating to node i within a boundary or finite element
$\mathbf{\Phi}$	Matrix of shape functions
$\mathbf{\Phi}^j$	Matrix of shape functions for element j
σ_x, σ_y	Principal components of stress
τ_{xy}	Shear stress component
ρ	Mass density
ω	Angular frequency
Ω	Domain for BE formulation
$\mathbf{C}$	FE global damping matrix
$\mathbf{C}^j$	Element damping matrix
c_1	Phase velocity of propagation of dilatational waves
c_2	Phase velocity of propagation of shear waves
$\mathbf{D}$	Stress-strain matrix
E	Young's modulus
f^j	Vector of nodal forces on element j
F_{ibe}	Vector of applied nodal forces on boundary element domain *ibe*
$\mathbf{G}$	Formulation matrix derived from displacement Green's function on a boundary element domain

G^{ij}	Terms of formulation matrix for a boundary element domain
$\mathbf{G}_{ibe}$	Formulation matrix for BE domain *ibe*
$\mathbf{G}^{I}_{ibe}$	The part of the BE formulation matrix relating to degrees of freedom at the interface with the FE domain
$\mathbf{G}^{R}_{ibe}$	The part of the BE formulation matrix relating to degrees of freedom not at the interface with the FE domain
$\mathbf{H}$	Formulation matrix derived from traction Green's function on a boundary element domain
$\mathbf{H}_{ibe}$	Formulation matrix for BE domain *ibe*
$\mathbf{H}_R$	Remainder of $\mathbf{H}$ after $\mathbf{H}_S$ is subtracted from it
$\mathbf{H}_S$	Part of $\mathbf{H}$ relating to the elastostatic solution
$\mathbf{H}^{I}_{ibe}$	The part of the BE formulation matrix relating to degrees of freedom at the interface with the FE domain
$\mathbf{H}^{R}_{ibe}$	The part of the BE formulation matrix relating to degrees of freedom not at the interface with the FE domain
$\hat{H}^{ij}$	Terms of formulation matrix for a boundary element domain without principle value terms absorbed
$\hat{\mathbf{H}}$	Boundary element formulation matrix before principle value terms are absorbed into its definition
i	When used as a superscript, denotes value at point location i
ibe	Index of BE domain
j	When used as superscript, element index, otherwise square root of -1
$\mathbf{K}$	FE global stiffness matrix
$\mathbf{K}^{j}$	Element stiffness matrix
K_0, K_1, K_2	Modified Bessel functions of the second kind and of zero, first and second order
k_1	Wave number of dilatational waves
k_2	Wave number of shear waves
$\mathbf{K}_{FE}$	FE dynamic stiffness matrix
$\mathbf{K}_{ibe}$	Equivalent finite element stiffness matrix for boundary element domain *ibe*
$\mathbf{K}^{I}_{FE}$	The part of the FE dynamic stiffness matrix relating to degrees of freedom at the interface with the FE domain
$\mathbf{K}^{R}_{FE}$	The part of the FE dynamic stiffness matrix relating to degrees of freedom not at the interface with the FE domain
$\mathbf{L}$	Matrix of spatial derivative operators, *i.e.* stress-displacement matrix
l, k	Direction indices
$\mathbf{M}$	FE global mass matrix
$\mathbf{M}^{j}$	Element mass matrix

$\mathbf{n}$	Unit vector normal to the boundary
N	Number of nodes in boundary element domain
N_B	Number of degrees of freedom in the BE domain
N_{BR}	Number of degrees of freedom in the BE domain not at the interface with the FE domain
NE	Number of elements in boundary element domain
N_F	Number of degrees of freedom in the FE domain
N_{FR}	Number of degrees of freedom in the FE domain not at the interface with the BE domain
P	Vector of tractions global to a boundary element domain
P^I	The vector of nodal tractions at the interface between the FE and BE domains
p_k	Traction in the direction k
p^*_{lk}	Solution for the traction in direction l resulting from a unit displacement applied at a point elsewhere applied in direction k (Green's function).
P^R_{ibe}	The vector of nodal tractions on the BE domain not the interface between the FE and BE domains
P^R_{FE}	The vector of nodal tractions on the FE domain not at the interface between the FE and BE domains
r	Radial distance between integration point on boundary and solution point i for the Green's functions
$\mathbf{s}$	Stress vector
$\mathbf{T}$	Transformation matrix from applied nodal tractions to applied nodal forces
$\mathbf{T}^R_{FE}$	The part of the transformation matrix calculated for the FE domain relating to degrees of freedom not at the interface with the FE domain
$\mathbf{T}^I_{FE}$	The part of the transformation matrix calculated for the FE domain relating to degrees of freedom at the interface with the FE domain
$\underline{u}$	Displacement vector
$\mathbf{u}$	Vector of displacement
u	'Pseudo-resultant' displacement amplitude response
u^j	Vector of nodal displacement values on element j
$\mathbf{u}^j$	Vector of displacement defined over element j
u, v, w	Components of displacement $\underline{u}$ in the x, y, z directions
u_k	Displacement in the k direction
u^*_{lk}	Solution for the displacement in direction l resulting from a unit traction applied at a point elsewhere applied in direction k (Green's function)
u^i_l	Displacement in direction l at point location i
U	Vector of displacements global to a boundary element domain

U^I	The vector of nodal displacements at the interface between the FE and BE domains
U^R_{ibe}	The vector of nodal displacements on the BE domain not at the interface between the FE and BE domains
U^R_{FE}	The vector of nodal displacements on the FE domain not at the interface between the FE and BE domains
x, y, z	Co-ordinate directions
x_l	Basis vector for direction l

1. INTRODUCTION

Trains running on lines on the ground surface produce vibration with predominant frequencies between about 4 Hz and 50 Hz. The Boundary Element Method (BEM) has been used previously to model the transmission of vibration in this frequency range for arbitrary geometry of the ground layers [1] and also to study the possible reduction of vibration transmission using stiffened soil structures [2]. The BEM is advantageous compared with other techniques because it is able to cope with features of arbitrary geometry such as ditches, embankments and cuttings while also modelling an infinite domain so that a regime of wave propagation is modelled [3]. The work of [1] and [2] used single-noded boundary elements on each of which the displacement was modelled as having a constant value. This approach demands that elements should be very much smaller than a wavelength of the waves in the solid and is adequate for low frequencies.

The present work is concerned with higher frequency vibration from trains that gives rise to structure borne or 'ground-borne' noise. This phenomenon is especially associated with trains running in cut-and-cover or bored tunnels although it has also been associated with trains running on surface tracks [4, 5]. Ground-borne noise has dominant frequency components from about 30 Hz to 200 Hz. The objectives in the present development of theoretical models therefore includes the modelling of tunnels and cuttings and the capability, with reasonable computing resources, to model waves of short wavelength covering this frequency range. The single-noded elements of [1] and [2] would require impracticable computing resources to cover this frequency range for meaningful analyses.

Already, within the present project, a computer program has been written to implement a two-dimensional boundary element (BE) model for elastodynamics. It has been shown using this that the boundary element method using three-noded elements with quadratic shape functions is capable of modelling vibration in realistic soils efficiently for a domain consisting of a single material [6]. However, for a model capable of including structures such as a tunnel lining or retaining walls, it is desirable that the BE method be combined with the use of finite elements (FE) in parts of the model. In the present work, therefore, a combined BE/FE method is considered.

This report presents the theory implemented in a suite of computer programs called TEA (Two-dimensional Elastodynamic Analysis). Some alternatives to the approach implemented in the software are also discussed. The software itself, and its use, are described in a separate report [7]. In [7] example analyses are presented for the special cases of a homogeneous half-space and a simple layered ground and these results are compared with a semi-analytical model in order to validate the FE/BE method and to study the nature of the numerical error incurred.

Dominguez [8] sets out a scheme for boundary element analysis for elastodynamics that has been followed in the present work. The method is outlined here in Section 2. This method has been implemented but greater formalism, adopted from the finite element approach, has been used in the definition of the data structures, particularly concerning element topology. A further modification to the method is required to enable the formulation to be used for open domains. This allows the infinite surface of the ground to be modelled using a finite number of boundary elements defined to a finite distance beyond the response positions of interest in the model. The method by which the equations may be formulated under these circumstances is given in Section 2.3.

The formulation of finite element matrices is well known. The isoparametric method used in the present model to derive the element mass, stiffness and damping matrices is standard but for the sake of recording the detail of the model without ambiguity is set out in outline in Section 3.

A number of alternative methods have been studied for coupling the finite element equations which are formulated in terms of nodal forces and the boundary element matrices which are formulated in terms of boundary tractions. Mustoe [9] sets out a number of alternative methods for static elastic analysis. Seven different methods are compared for computational efficiency and accuracy by Tullberg *et al.* [10]. On the grounds of the conclusions of that work two methods are discussed in Section 4 of the present report. The reasons for the choice of method implemented in the software described in [6] is explained in Section 4.4

Finally, in Sections 5 and 6, two case examples are presented. The first of these is a bored tunnel for which the effect of including a concrete lining is investigated. The second example is a twin track, cut-and-cover tunnel with and without stiffened foundations to the abutment walls. The examples are used to show how results from the model may be used in practice.

2. THE FORMULATION FOR A BOUNDARY ELEMENT DOMAIN

2.1 Outline of theory

Consider a body Ω with a surface Γ (Figure 1). If time-harmonic solutions are assumed, *i.e.* seeking a formulation for the frequency domain, the displacement at a point i on the body, in a direction defined by the basis vector x_l, is described by the complex amplitude of displacement u_l^i times $e^{j\omega t}$ which represents the assumed time-harmonic variation of the forces and displacements.

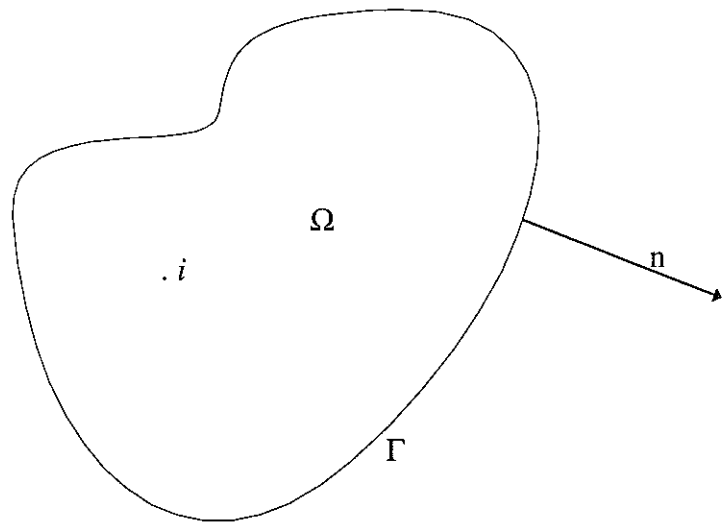

Figure 1. The domain Ω with surface Γ.

Dropping the $e^{j\omega t}$ terms, the harmonically reduced formulation is stated by the integral equation for elastodynamics as [8]

$$u_l^i + \int_\Gamma \sum_k p_{lk}^* u_k \, d\Gamma = \int_\Gamma \sum_k u_{lk}^* p_k \, d\Gamma \qquad (1)$$

where u_k is the complex amplitude of displacement at a point on the surface Γ in the direction of the basis vector k and p_k is a traction at a point on the surface Γ in the k direction. The tensor p^*_{lk} represents the solution for the traction in the l direction at the interior point i arising from a unit applied displacement at a surface point in the direction k. Likewise, u^*_{lk} represents the solution for the displacement in the l direction at i due to a unit load at the point on the boundary in the k direction. These are known as the Green's function solutions. (The superscript * is used here to distinguish these functions from the state variables p and u.) In performing the integration, the surface point is "moved" around Γ. For the two-dimensional case, the unit solutions p^*_{lk} and u^*_{lk} are 2 by 2 tensors (indicated by the subscripts each taking two basis vector directions). The elements of these tensors are functions of the distance between the surface point and the point i. The integral equation, as stated here in terms only of integrals over the surface, assumes that all loads are applied on the boundary and none are applied within the volume of Ω.

The integral equation for the elastodynamic wave field, equation (1), is similar in form to the Kirchhoff-Helmholz integral equation that represents an acoustic wave field and that can be derived from the scalar wave equation. Similarly the integral equation for elastodynamics can be derived from the Navier's differential equations [8]. The Navier's equations for elastodynamics are

$$\begin{aligned}(\lambda+\mu)\frac{\partial\Delta}{\partial x}+\mu\nabla^2 u &= \rho\frac{\partial^2 u}{\partial t^2}\\ (\lambda+\mu)\frac{\partial\Delta}{\partial y}+\mu\nabla^2 v &= \rho\frac{\partial^2 v}{\partial t^2}\\ (\lambda+\mu)\frac{\partial\Delta}{\partial z}+\mu\nabla^2 w &= \rho\frac{\partial^2 w}{\partial t^2}\end{aligned} \qquad (2)$$

where ρ is the density of the material, u, v, w are the x, y, z components of displacement $\underline{u}$, $\Delta = \frac{\partial u}{\partial x}+\frac{\partial v}{\partial y}+\frac{\partial w}{\partial z}$ and

$$\lambda = \frac{\nu E(1+i\eta)}{(1+\nu)(1-2\nu)}, \quad \mu = \frac{\nu E(1+i\eta)}{2(1+\nu)}$$

are the Lamé constants where E is the Young's modulus, ν is the Poisson's ratio and η is the loss factor representing the material damping of the body.

The theory is now developed for the solution of wave propagation of in-plane motion in the xy plane. For two-dimensions, the Green's function tensors u^*_{lk} and p^*_{lk} are

$$u^*_{lk} = \frac{1}{2\pi\rho c_2^{\,2}}[\psi\delta_{lk} - \chi\frac{\partial r}{\partial x_l}\frac{\partial r}{\partial x_k}] \qquad (3)$$

and

$$p_{lk}^{*} = \frac{1}{2\pi}\left[\left(\frac{d\psi}{dr}-\frac{1}{r}\chi\right)\left(\delta_{lk}\frac{\partial r}{\partial n}+\frac{\partial r}{\partial x_k}n_l\right)-\frac{2}{r}\chi\left(n_k\frac{\partial r}{\partial x_l}-2\frac{\partial r}{\partial x_l}\frac{\partial r}{\partial x_k}\frac{\partial r}{\partial n}\right)\right.$$
$$\left.-2\frac{d\chi}{dr}\frac{\partial r}{\partial x_l}\frac{\partial r}{\partial x_k}\frac{\partial r}{\partial n}+\left(\frac{c_1^{\,2}}{c_2^{\,2}}-2\right)\left(\frac{d\psi}{dr}-\frac{d\chi}{dr}-\frac{1}{r}\chi\right)\frac{\partial r}{\partial x_l}\frac{\partial r}{\partial x_k}\right] \tag{4}$$

where δ_{lk} is the Kroneker delta function, **n** is the unit external normal vector at the surface (with components n_k and n_l), r is the distance between the source and observation points, c_1 is the velocity of dilatational waves (P-waves) and c_2 is the shear (S-wave) velocity in the solid. These are calculated from the density ρ, and the Lamé constants λ and μ as

$$c_1^{\,2} = \frac{\lambda+2\mu}{\rho} \quad c_2^{\,2} = \frac{\mu}{\rho} \tag{5}$$

and in general are complex values, the imaginary parts of which represent the material damping of the medium. The terms ψ and χ in equations (3) and (4) are given by

$$\psi = K_0(k_2 r)+\frac{1}{k_2 r}\left[K_1(k_2 r)-\frac{c_2}{c_1}K_2(k_1 r)\right] \tag{6}$$

and

$$\chi = K_2(k_2 r)-\frac{c_2}{c_1}K_2(k_1 r) \tag{7}$$

in which $k_1 = \omega/c_1$ and $k_2 = \omega/c_2$ are the dilatational wave number and shear wave number, respectively and K_0, K_1, K_2 are modified Bessel functions of the second kind and of zero, first and second order.

2.2 Discretization

Following the general development of the BEM, the next step is to take the point i to the surface Γ. This leads to

$$\varepsilon^i\begin{Bmatrix} u_x^{\,i} \\ u_y^{\,i}\end{Bmatrix}+\int_\Gamma \sum_k p_{lk}^{*}\,u_k\,d\Gamma = \int_\Gamma \sum_k u_{lk}^{*}\,p_k\,d\Gamma \tag{8}$$

where $\varepsilon^i = \begin{bmatrix} \frac{1}{2} & 0 \\ 0 & \frac{1}{2}\end{bmatrix}$ when the boundary at point i is smooth.

Equation (8) is the boundary integral equation to which, as for the acoustic case, the boundary element discretization and collocation method is applied. When the surface point is taken at the location of the point i, the Green's function tensors contain infinite terms and this must be dealt with in the integration process.

In the program TEA only a single type of boundary element has been implemented; it has three nodes and uses quadratic shape functions. The element is illustrated in Figure 2.

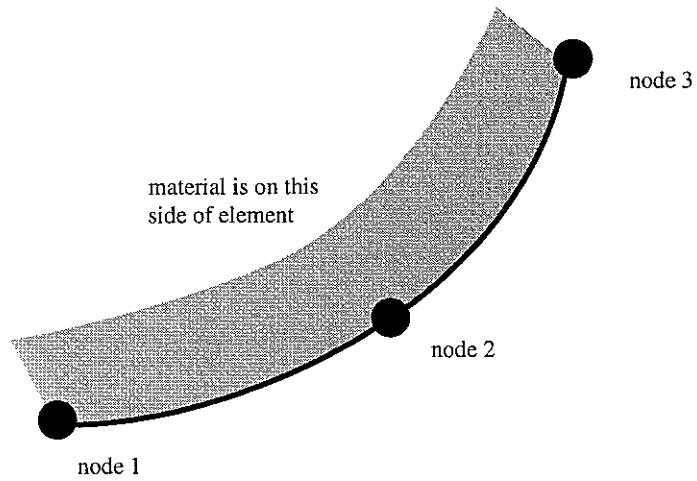

Figure 2. Three-noded, quadratic shape function element.

The process of discretization of the BE formulation uses the finite element approximation method for the functions u and p over the surface as well as to approximate the geometry of the surface from the nodal co-ordinates. For example for a piont at ξ on the jth element,

$$\mathbf{u}(\xi) = \begin{Bmatrix} u_x(\xi) \\ u_y(\xi) \end{Bmatrix} = \Phi(\xi) u^j = \begin{bmatrix} \phi_1 & 0 & \phi_2 & 0 & \phi_3 & 0 \\ 0 & \phi_1 & 0 & \phi_2 & 0 & \phi_3 \end{bmatrix} \begin{Bmatrix} u_x^1 \\ u_y^1 \\ u_x^2 \\ u_y^2 \\ u_x^3 \\ u_y^3 \end{Bmatrix} \tag{9}$$

where $\phi_1 = \frac{1}{2}\xi(\xi - 1)$, $\phi_2 = (1 - \xi^2)$, $\phi_3 = \frac{1}{2}\xi(\xi + 1)$ and $-1 \le \xi \le 1$, ξ being the non-dimensional internal co-ordinate defining any point within the element.

For a single point i, the discretized boundary equation is

$$\varepsilon^i u^i + \sum_{j=1}^{NE} \left\{ \int_{\Gamma_j} p^* \Phi \, d\Gamma \right\} \mathbf{u}^j = \sum_{j=1}^{NE} \left\{ \int_{\Gamma_j} u^* \Phi \, d\Gamma \right\} \mathbf{p}^j \tag{10}$$

where NE is the number of elements and $\mathbf{u}^j$ and $\mathbf{p}^j$ are vectors of nodal values of u and p for the element. u^* and p^* are now 2×6 matrices of terms relating the component directions at the 3 nodes of element j to those at i.

For a system of elements with a total of N nodes, equation (10) has the form

$$\varepsilon^i u^i + \left[\hat{H}^{i1} \quad \hat{H}^{i2} \quad .. \quad \hat{H}^{iN}\right] \begin{Bmatrix} u_x^1 \\ u_y^1 \\ u_x^2 \\ u_y^2 \\ . \\ . \\ u_x^N \\ u_y^N \end{Bmatrix} = \left[G^{i1} \quad G^{i2} \quad .. \quad G^{iNE}\right] \begin{Bmatrix} \mathbf{p}^1 \\ \mathbf{p}^2 \\ \mathbf{p}^3 \\ . \\ . \\ . \\ . \\ \mathbf{p}^{NE} \end{Bmatrix} \tag{11}$$

Notice that here the element matrices, $\hat{H}^{ij}$ are assembled in the finite element sense, *i.e.* the terms for the nodes common to neighbouring elements are added into the global matrix.

In Dominguez's method [8] for a single domain, the terms of the **G** matrix are not added together but kept separately. In [6] this allowed the column vector of tractions $\{p\}$ to maintain two separate values at a single node and thus to model discontinuous applied tractions at the boundary. Here, however, it is necessary to assemble **G** in the same way as **H** as the coupling between two boundary element domains, or between a finite element domain and a boundary element domain, requires that the model carry only a single common value of force/traction at each node at the interface. In the boundary element formulation this imposes the assumption that the traction in the x and y directions are continuous functions around the boundary of the domain. This clearly is not the case where there is a corner at the junction of two boundary elements, as in this case the normal vector on the two elements represents a discontinuous direction in which a stress (arbitrary direction) is resolved to form the x and y direction tractions.

In the present implementation this difficulty is avoided by transforming the boundary element matrices to equivalent FE matrices which are specified in terms of the loads applied as point forces at the nodes. The method for this and the coupling to an FE region are given later in Section 4.

Returning to the development of the BE system matrices, by allowing the point i to take the position of each node in turn and assembling both **H** and **G** from the row matrices of equation (11), a full set of equations is obtained in the form,

$$\underset{(N\times N)}{\mathbf{H}} \quad \underset{(N\times 1)}{U} \quad = \quad \underset{(N\times N)}{\mathbf{G}} \quad \underset{(N\times 1)}{P} \tag{12}$$

where U and P are the vectors of nodal displacements and tractions for the boundary element domain. The definition of **H** now absorbs the $\hat{H}^{ij}$ terms and the ε^i terms on the diagonal.

2.3 Evaluation of singular integral terms

In constructing the global equation (12) the integrals in equation (10) are evaluated for the Green's functions on each element making up the total integration around the boundary. For most of the elements, by using the finite-element type mapping of the element using the shape functions, the integral can be calculated using a standard numerical integration method. In the

present case a 10 point Gauss-Legendre quadrature rule is used. The high order of this quadrature reflects the high polynomial order of the integrand.

When the collocation node, i, is on the element j the integrand becomes singular for both the evaluation of $\hat{\mathbf{H}}$ and $\mathbf{G}$. The singular terms of the $\mathbf{G}$ matrix may be integrated using a special quadrature rule that takes into account the presence of a weak singularity which is of logarithmic order. The singularity in the $\hat{\mathbf{H}}$ term, however, is of the order $1/r$ and is not integrable. The reason that the total integration round the boundary for these terms has a finite result is that the integrand has singular terms of opposite signs either side of each node and these cancel. The implication of this is that the diagonal terms of the $\mathbf{H}$ matrix cannot be evaluated using any quadrature scheme on an element by element basis and an alternative method must be used to evaluate the principal value of the integral through these nodes indirectly.

Following reference [8], for a closed boundary, the difficulty in calculating the diagonal terms of $\mathbf{H}$ can be overcome by splitting the evaluation of the $\mathbf{H}$ integrand at the Green's function level into two parts so that, $\mathbf{H} = \mathbf{H}_S + \mathbf{H}_R$ the first part, $\mathbf{H}_S$, representing the static elasticity case, and the second, $\mathbf{H}_R$, making up the rest of the value of the Green's function for the dynamic case at the solution frequency. This is achieved by expanding the functions K_0, K_1, K_2 as a series in kr and collecting the terms which correspond to the Green's function for the elastostatics problem [8]. The singular part of the $\mathbf{H}$ terms is related only to the static case and therefore only has to be evaluated in $\mathbf{H}_S$ once and can then be used for analyses at many frequencies. The separated-off terms, $\mathbf{H}_R$, that complete the dynamic terms of $\mathbf{H}$ contain no singularity and can therefore be evaluated using the standard Gauss-Legendre quadrature.

For the static case, a static rigid body motion, for example represented by a vector U containing ones in all the u_x terms, (or the equivalent in the y direction) must be associated with zero applied loads around the boundary (see equation (12)). This implies that the sum of the row of terms of $\mathbf{H}_S$ for either degree of freedom at each node i must be zero and the diagonal term can be evaluated as.

$$H_s^{ii} = \varepsilon^i + \hat{H}_s^{ii} = -\sum_{nodes j \neq i} \hat{H}_s^{ij} \tag{14}$$

This method evaluates the singular integral term and the value of ε^i simultaneously and is therefore efficient in dealing with the case of node i being at a corner, rather than at a smooth part of the boundary, when $\varepsilon^i \neq \begin{bmatrix} \frac{1}{2} & 0 \\ 0 & \frac{1}{2} \end{bmatrix}$.

In the present work a method is required that deals with boundaries which are left open so that an infinite boundary can be approximated. It has already been stated that the singular integral terms of the $\mathbf{H}$ matrix cannot be dealt with by integrating element by element. A method has therefore been devised to deal with this. In this each pair of elements is taken in turn and a small closed boundary is constructed by adding a small number of new elements to the pair of elements (Figure 3). It has been found that 5 extra elements are sufficient, making each closed boundary 7 elements (see below).

The terms H_s^{ii} are evaluated using the method implied by equation (14) for the mid-nodes of the two original elements and the node in common between them and stored for use in the matrix equation for the full boundary later on. This method is valid since the terms may be seen as dependent only on the integration over the elements to which the node *i* belongs and are therefore independent of the new 'false' boundary that is set up temporarily. The method is efficient since although setting up the **H** matrix for NE boundaries of 7 elements is required, this is fast compared to the setting up of the rest of **H** for the complete boundary where NE is much larger than 7. The process of determining the terms H_s^{ii} need only be carried out once and the results can be used to set up the global matrices for solutions at all frequencies required thereafter.

It is possible for the construction of the small boundary to introduce significant error at a pair of elements for certain geometries where a combination of the three following conditions apply

- contiguous elements differ greatly in length
- an angle close to 2π exists between the two elements
- either of the elements is strongly curved.

Since these conditions would, in any case, represent poor practice in discretizing a BE model for a wave propagating problem, the fact that this method would produce poor results under these circumstances should not cause a difficulty in practice. In fact the method has been tested and found to be stable and accurate in the evaluation of the singular terms for a wide variety of possible element geometries. Very little improvement occurs if more than 5 new elements are chosen to complete the closed boundary.

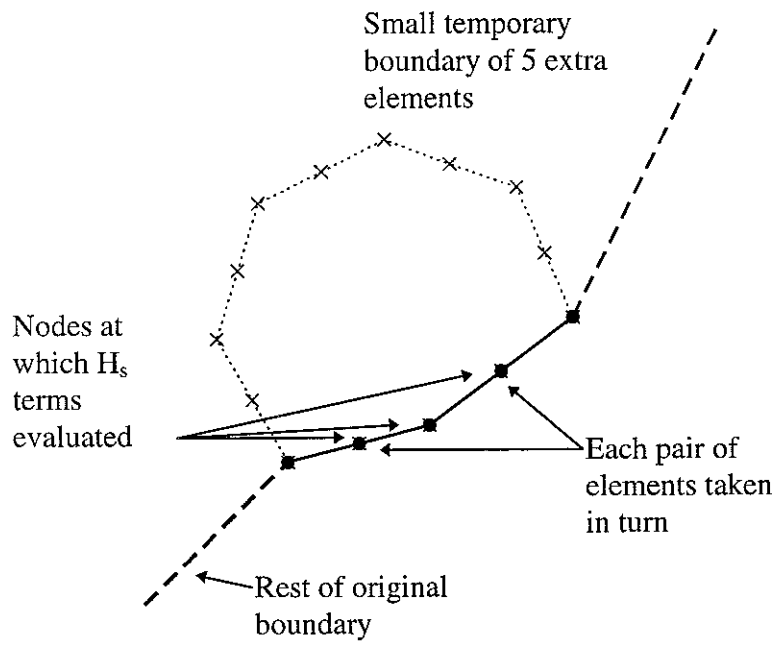

Figure 3. Small boundary constructed around each pair of elements.

Nodes on the 'loose' ends of a boundary, where it has been left open to approximate an infinite boundary, have been allotted the value $\varepsilon^i = \begin{bmatrix} \frac{1}{2} & 0 \\ 0 & \frac{1}{2} \end{bmatrix}$ and $\hat{H}_s^{ii} = \mathbf{0}$. This imposes the assumed condition that, at this point, the boundary is smooth and that the elements either side of this node (implied) are straight lines. Since the ends of the boundary should be at a distance from the region where a solution is required, this should cause no difficulty in practice.

2.4 Division of the model into sub-domains

In summary, the formulation has been derived up to the point at which it is shown how the matrices are constructed representing a boundary element model of a domain consisting of a single homogeneous material. A model for a layered ground with arbitrary geometry of the ground surface and interfaces, which may also incorporate built structures, can be constructed from a number of such boundary elements. For each boundary element domain the matrices $\mathbf{H}_{ibe}$ and $\mathbf{G}_{ibe}$, where the subscript *ibe* is used to denote a domain number, can be constructed separately using the procedure described in Sections 2.1 to 2.3. For boundary elements to be used in this way the structure must be divisible into a number of homogeneous domains. Apart from their common boundary their surfaces must not be close to one another as this leads to error in the quadrature process [6].

For thin structures with more detailed geometry and with components of differing materials a finite element model is appropriate. The formulation has therefore been extended to provide for finite elements to be coupled with an arbitrary number of boundary element domains to form the complete coupled model for the ground and built structures. Finite element theory is well known, but, for the purposes of defining the terms and specifying exactly what is implemented in the software of [7], the derivation of the system matrices for a finite element model is described concisely in Section 3.

Once the matrices for the boundary element domains and finite elements of the model have been calculated they are assembled into a global dynamic stiffness matrix. The excitation of vibration is defined in terms of applied nodal forces and the system is solved for the unknown displacement responses at all nodes of the model. The assembly and solution process is straightforward and not described further in the present report although the details concerning the software structure by which this process is achieved using the computer memory efficiently is described in [7].

3. THE FORMULATION FOR A FINITE ELEMENT DOMAIN

Define the terms

$$\mathbf{L}=\begin{bmatrix}\dfrac{\partial}{\partial x} & 0\\ 0 & \dfrac{\partial}{\partial y}\\ \dfrac{\partial}{\partial y} & \dfrac{\partial}{\partial x}\end{bmatrix},\qquad \mathbf{s}=\begin{bmatrix}\sigma_x\\ \sigma_y\\ \tau_{xy}\end{bmatrix},\qquad \mathbf{u}=\begin{bmatrix}u_x\\ u_y\end{bmatrix} \tag{15}$$

where σ_x, σ_y and τ_{xy} are the components of the stress **s**, **u** is the displacement (as in Section 2) and **L** is a matrix of spatial differential operators.

For the plane strain condition the stress-strain relation (Hooke's law) may now be stated as

$$\begin{bmatrix}\sigma_x\\ \sigma_y\\ \tau_{xy}\end{bmatrix}=\frac{E(1-\nu)}{(1+\nu)(1-2\nu)}\begin{bmatrix}1 & \dfrac{\nu}{(1-\nu)} & 0\\ \dfrac{\nu}{(1-\nu)} & 1 & 0\\ 0 & 0 & \dfrac{(1-2\nu)}{2(1-\nu)}\end{bmatrix}\begin{bmatrix}\varepsilon_x\\ \varepsilon_y\\ \gamma_{xy}\end{bmatrix} \tag{16}$$

or

$$\sigma=\mathbf{D}\varepsilon \tag{17}$$

where E is the Young's modulus and ν is the Poisson's ratio of the material. ε_x, ε_y, and γ_{xy} are the strain components given by the strain-displacement relationship

$$\begin{bmatrix}\varepsilon_x\\ \varepsilon_y\\ \gamma_{xy}\end{bmatrix}=\begin{bmatrix}\dfrac{\partial}{\partial x} & 0\\ 0 & \dfrac{\partial}{\partial y}\\ \dfrac{\partial}{\partial y} & \dfrac{\partial}{\partial x}\end{bmatrix}\begin{bmatrix}u_x\\ u_y\end{bmatrix} \tag{18}$$

or

$$\varepsilon=\mathbf{L}\,\mathbf{u} \tag{19}$$

To implement the finite element method, the structure is divided into finite elements and the displacement on each element is approximated using shape functions. This approach is the same as that for approximating the displacement over a boundary element that has already been described in Section 2.2. Hence the displacement is approximated as

$$\mathbf{u}=\Phi u^j \tag{20}$$

where u^j is the vector of nodal displacements on element j. Φ is the matrix of shape functions for each node and degree of freedom of the element.

The kinetic energy ('½ $m v^2$') and the strain energy ('½ $k x^2$') integrated over the element can be evaluated as

$$T = \frac{1}{2}\iint \dot{u}^{jT}\Phi^T\rho\Phi\dot{u}^j \, dx\, dy \text{ and } U = \frac{1}{2}\iint u^{jT}(\mathbf{L}\Phi)^T\mathbf{D}\mathbf{L}\Phi u^j \, dx\, dy \quad (21)$$

respectively. Using the Lagrange equation (derived, for instance, in reference [11])

$$\frac{d}{dt}\left(\frac{\partial T}{\partial \dot{u}}\right) + \frac{\partial U}{\partial u} = f \quad (22)$$

where f represents the applied forces, the differential equation governing the deformation of an element may be stated as

$$\mathbf{M}^j\ddot{u}^j + \mathbf{K}^j u^j = f^j \quad (23)$$

where f^j represents the element nodal forces and

$$\mathbf{M}^j = \iint \Phi^T\rho\Phi \, dx\, dy \quad (24)$$

$$\mathbf{K}^j = \iint (\mathbf{L}\Phi)^T\mathbf{D}\mathbf{L}\Phi \, dx\, dy \quad (25)$$

The integration to form these matrices is performed numerically using Gauss-Legendre quadrature. The finite element method uses the shape function approximation method to map the shape of the element from the co-ordinates of its nodes onto a generic element for this process. Thus the shape functions are used to approximate the geometry of the element as well as the displacement function over it. In the ground vibration model four elements have been implemented. These are: a three-noded triangular element with linear shape functions, a four-noded quadrilateral element with linear shape functions, a six-noded triangle element with quadratic shape functions and an eight-noded quadrilateral element with quadratic shape functions (see [7]).

The displacements are assumed to be harmonic in time with circular frequency ω, and u^j and f^j are now used to represent the complex amplitudes of displacement and load at the nodes of the element as for the boundary element case in Section 2. The differential equation for an element reduces to

$$(-\mathbf{M}^j\omega^2 + \mathbf{K}^j)\, u^j = f^j \quad (26)$$

No damping is represented in the equations at this stage. Damping can be introduced to the model by means of a loss factor specified for the material of the element. By this means an element damping matrix is directly produced using the element stiffness matrix $\mathbf{K}^j$. Hence

$$(-\mathbf{M}^j\omega^2 + i\mathbf{C}^j + \mathbf{K}^j)\, u^j = f^j \quad (27)$$

where

$$\mathbf{C}^j = \eta \mathbf{K}^j \tag{28}$$

The assembly to form a mass, damping and stiffness matrix for the complete finite element domain is carried out by adding terms from all elements which pertain to the same degrees of freedom of the model. This produces the domain matrices **M**, **C** and **K** for the finite element part of the overall model. For a single frequency ω it is convenient to reduce this system of matrices using the global form of equation (27) to a single dynamic stiffness matrix $\mathbf{K}_{FE}$ to represent the formulation for the finite element domain of the model. Hence

$$(-\mathbf{M}\omega^2 + i\mathbf{C} + \mathbf{K})\, u = \mathbf{K}_{FE}\, u = f \tag{29}$$

Note that although **K**, **C** and **M** can be derived once and used for all frequencies, the equivalent boundary element matrices are frequency dependent and have to be recalculated at each frequency step.

The vector of nodal forces is not constructed until after the coupling between the finite element domain and the boundary element domains of the model is achieved.

4. COUPLING BE AND FE MATRICES

4.1 Introduction

This section describes how the matrix $\mathbf{K}_{FE}$, representing the finite elements of the model, and the matrices $\mathbf{G}_{ibe}$ $\mathbf{H}_{ibe}$, ibe = 1, 2, .., representing the boundary element domains, are coupled to form a system of equations representing the entire model for a given frequency ω. The coupling is established on the basis of continuity of displacement at the common nodes between the sub-domains and on the basis of equilibrium of forces at the interfaces. The forces at the interfaces are described, however, in different ways for a finite element domain and for a boundary element domain. The finite element matrices are formulated in terms of applied point forces at the nodes. The boundary element matrices are formulated on the basis of applied tractions distributed over the line of the element. This leads to two approaches for coupling the BE and FE matrices. In both it is assumed that the nodes of the neighbouring BE and/or FE sub-domains coincide.

1. The coupling may be carried out by transforming the boundary element matrices to form a dynamic stiffness matrix in terms of equivalent nodal forces.
2. The coupling may be carried out on the basis of equilibrium of tractions on the interfaces. For this the FE dynamic stiffness matrix must be transformed to one in terms of tractions on the boundary.

The first of these options has been implemented in the software developed in the present project. This allows the resulting dynamic stiffness matrices to be assembled in the finite element sense and for the response of the whole model to applied nodal forces to be calculated. The method is explained in Section 4.2. The second approach has computational advantages but does not provide a simple means of dealing with the problem of coupling at points where the implied tractions are discontinuous. Although it has not been applied in the present work the method is described in Section 4.3 for future reference.

4.2 Conversion of the BE matrices to an equivalent FE matrix

Consider a single finite, or boundary, element on which tractions are applied. The work done by the applied tractions $\mathbf{p}$ in applying a virtual displacement $\delta\mathbf{u}$ at the boundary Γ_j of the element is (force times displacement)

$$\delta w = \int_{\Gamma_j} \delta\mathbf{u}^T \mathbf{p}\, d\Gamma \tag{30}$$

Using the element shape functions to interpolate the displacement and the tractions on the element surface in terms of the vectors u^j and p^j of nodal displacements and nodal traction values so that $\mathbf{u} = \Phi u^j$ and $\mathbf{p} = \Phi p^j$ as before gives

$$\delta w = \left\{\delta u^j\right\}^T \int_{\Gamma^j} \Phi^T \Phi d\Gamma\ p^j \tag{31}$$

This equates to the virtual work done by the equivalent nodal forces f^j that would be applied to achieve the same virtual displacement values, δu^j, at the nodes. That is,

$$\delta w = \left\{\delta u^j\right\}^T f^j \tag{32}$$

Comparing Equations (32) and (31) gives

$$f^j = \int_{\Gamma_j} \Phi^T \Phi\, d\Gamma\ p^j \tag{33}$$

This provides a matrix expression, calculated from the shape functions for the elements at which p^j is applied, that transforms the vector of applied tractions into a vector of applied nodal forces.

Calculating the element transformation matrices represented by the integral in Equation (33) for all the boundary elements of a boundary element domain and assembling them into a global system for the domain yields a transformation matrix [**T**] such that

$$\{F\} = [\mathbf{T}]\ \{P\} \tag{35}$$

where {F} is a vector of nodal forces equivalent to the tractions {P} applied on the domain.

As [**T**] is to be constructed for a domain modelled using boundary elements there is no difficulty in identifying the elements and nodes to which the process of constructing [**T**] should be applied as all the nodes of all elements of the boundary element domain are involved.

If the matrix [**T**] for a particular domain is denoted $\mathbf{T}_{ibe}$, premultiplying Equation (12) by $\mathbf{T}_{ibe}(\mathbf{G}_{ibe})^{-1}$ gives

$$\left[\mathbf{T}_{\text{ibe}}(\mathbf{G}_{\text{ibe}})^{-1}\mathbf{H}\right]\{U_{ibe}\} = \mathbf{T}_{\text{ibe}}\{P_{ibe}\} = \{F_{ibe}\} \tag{36}$$

which defines $\left[\mathbf{T}_{\text{ibe}}(\mathbf{G}_{\text{ibe}})^{-1}\mathbf{H}\right] \equiv \mathbf{K}_{ibe}$ as the dynamic stiffness matrix for the BE domain which connects the nodal displacements to the forces applied at the nodes of the boundary element domain.

$\mathbf{K}_{ibe}$ for *ibe* = 1, 2, .. may therefore be assembled in the finite element sense along with $\mathbf{K}_{FE}$ into a global matrix system representing the entire model.

It should be noted that although a dynamic stiffness matrix, in some respects similar to a finite element dynamic stiffness matrix has been constructed, $\mathbf{K}_{ibe}$ does not have the properties of limited bandwidth or symmetry that an FE matrix has. Mustoe [9] suggests a method by which a symmetric boundary element stiffness matrix can be produced. Although the procedure for computing this is a little more complicated, this approach offers savings in terms of computer memory. However, the method requires the inversion of a matrix of twice the size of that found in the method described above. Tullberg and Bolteus [10] conducted a study of seven methods of deriving a stiffness matrix from the BE matrices which included the methods yielding asymmetric and symmetric dynamic stiffness matrices. They concluded that:

1. The direct asymmetric stiffness matrix, *i.e.* the method described above, is the best method in terms of accuracy.

2. The direct asymmetric stiffness matrix formed from BE matrices is as good as, or better than, an FE matrix with the same size elements in the discretization. This finding is upheld by investigations using the method by the present authors [7].

3. Methods leading to a symmetric equivalent FE matrix were found to have such poor accuracy that the authors did not think the saving of memory space was not a sufficient advantage to justify their use.

For these reasons the direct method of deriving an asymmetric matrix, described in this section, has been implemented in the program described in [7].

4.3 Conversion of the FE matrices to an equivalent BE matrix

An alternative approach to the coupling problem is to reformulate the finite element matrices as equivalent boundary element matrices and couple them by ensuring equilibrium of tractions on the element edges rather than of nodal forces. This is described below for future reference, although it is not used in the current software/project.

For the boundary element region *ibe* partition the matrix equation (12) as

$$\begin{bmatrix}\mathbf{H}^R_{ibe} & \mathbf{H}^I_{ibe}\end{bmatrix}\begin{bmatrix}U^R_{ibe}\\ U^I_{ibe}\end{bmatrix} = \begin{bmatrix}\mathbf{G}^R_{ibe} & \mathbf{G}^I_{ibe}\end{bmatrix}\begin{bmatrix}P^R_{ibe}\\ P^I_{ibe}\end{bmatrix} \tag{37}$$

where U^I_{ibe}, P^I_{ibe} are interface displacements and tractions and U^R_{ibe}, P^R_{ibe} relate to the remainder of the nodes.

For the finite element domain, similarly

$$\begin{bmatrix}\mathbf{K}_{FE}^{R} & \mathbf{K}_{FE}^{I}\end{bmatrix}\begin{bmatrix}U_{FE}^{R}\\ U_{FE}^{I}\end{bmatrix}=\begin{bmatrix}\mathbf{T}_{FE}^{R} & \mathbf{T}_{FE}^{I}\end{bmatrix}\begin{bmatrix}P_{FE}^{R}\\ P_{FE}^{I}\end{bmatrix} \tag{38}$$

where the transformation matrix **T** has been defined on the finite element domain.

The conditions of equilibrium and continuity of displacements is now satisfied by

$$\begin{aligned} U_{ibe}^{I} &= U_{FE}^{I} = U^{I} \\ P_{ibe}^{I} &= -P_{FE}^{I} = P^{I} \end{aligned} \tag{39}$$

Equation (37) can now be rearranged in the form

$$\begin{bmatrix}\mathbf{H}_{ibe}^{R} & \mathbf{H}_{ibe}^{I} & -\mathbf{G}_{ibe}^{I}\end{bmatrix}\begin{bmatrix}U_{ibe}^{R}\\ U^{I}\\ P^{I}\end{bmatrix}=\begin{bmatrix}\mathbf{G}_{ibe}^{R}\end{bmatrix}\begin{Bmatrix}P_{ibe}^{R}\end{Bmatrix} \tag{40}$$

and Equation (38) in the form

$$\begin{bmatrix}\mathbf{K}_{FE}^{R} & \mathbf{K}_{FE}^{I} & \mathbf{T}_{FE}^{I}\end{bmatrix}\begin{bmatrix}U_{FE}^{R}\\ U^{I}\\ P^{I}\end{bmatrix}=\begin{bmatrix}\mathbf{T}_{FE}^{R}\end{bmatrix}\begin{Bmatrix}P_{FE}^{R}\end{Bmatrix} \tag{41}$$

Equations (40) and (41) can be written together as one single matrix equation

$$\underset{(N_F+N_B)\times(N_F+N_B)}{\begin{bmatrix}\mathbf{H}_{ibe}^{R} & \mathbf{H}_{ibe}^{I} & -\mathbf{G}_{ibe}^{I} & \mathbf{0}\\ \mathbf{0} & \mathbf{K}_{FE}^{I} & \mathbf{T}_{FE}^{I} & \mathbf{K}_{FE}^{R}\end{bmatrix}}\begin{bmatrix}U_{ibe}^{R}\\ U^{I}\\ P^{I}\\ U_{FE}^{R}\end{bmatrix}=\underset{(N_F+N_B)\times(N_{FR}+N_{BR})}{\begin{bmatrix}\mathbf{G}_{ibe}^{R} & \mathbf{0}\\ \mathbf{0} & \mathbf{T}_{FE}^{R}\end{bmatrix}}\begin{bmatrix}P_{ibe}^{R}\\ P_{FE}^{R}\end{bmatrix} \tag{42}$$

in which the first column of the matrix on the left side consists of terms from the BE domain only, the second and third columns consist of terms for the interface and the fourth column has terms which solely relate to the FE domain. The dimensions of the matrices on the left and right of the equation are indicated using the symbols N_F, N_B, N_{FR} and N_{BR}, to represent the numbers of degrees of freedom of the finite element domain, of the boundary element domain, of the non-interface part of the finite element domain and the non-interface part of the boundary element domain respectively. If the tractions specified in the column vector on the right of equation (42) are known (notice that tractions may not be applied on the interface) this equation may be solved for the displacement vector (left side).

4.4 Choice of coupling method

The equivalent BE matrix method has been developed for the case of coupling a single FE and a single BE domain (Section 4.3). The complexity in implementing the method in a computer program is greater where an arbitrary number of boundary element domains is

involved, as is the required effort in data preparation, since the interface and non-interface nodes of the FE and BE domains must be identified, and the matrices repartitioned to introduce each new domain.

The BE matrix method has the advantage over the equivalent nodal forces method that there is no matrix inversion involved is producing the global system of equations. This is the step (equation (36)) which, for most practical problems, takes the greatest amount of computing time. The equivalent BE matrix method would therefore be considerably more time efficient. However, from equation (42) it can be seen that the equivalent BE matrix method requires more computer array storage space. It also carries the minor disbenefit that loads cannot be applied at the interfaces of the domains.

No method has been developed here to solve the problem of discontinuous tractions. This would involve the definition of multiple coincident nodes that would add extra rows to the matrix in a manner similar to the pure boundary element method described in [7]. For coupling to FE regions extra terms would have to be derived. Mustoe [8] outlines four methods of dealing with this problem. This would add considerable complexity to the implementation of this method as well as in its use. The method of expressing the BE matrices in terms of nodal forces avoids having to allow for discontinuous tractions at corners of the boundary element domain. In [7] it has been checked experimentally that this does not generate any spurious discontinuity in the displacement function through a corner of a BE domain connected directly to an FE domain and so this method has been found to be satisfactory.

In comparing the method of Section 4.3 with the stiffness matrix approach of Section 4.2, a judgement also arises as to whether it is most useful or convenient to enter the loads as tractions over finite lengths of boundary element, or finite element, edges or whether specification in terms of nodal forces is to be preferred.

These reasons have contributed to the decision to implement the boundary element stiffness matrix approach of Section 4.2 rather than the method described in Section 4.3.

5. EXAMPLE ANALYSIS - A BORED TUNNEL WITH AND WITHOUT CONCRETE LINING.

5.1 Model

In reference [7] the software 'TEA' that has been developed is described and instructions are provided on data preparation. In that report a number of analyses for a homogeneous half-space and for a simple layered half-space are presented. The results for these cases are compared to a semi-analytical model [12] through which the nature of the numerical error is investigated. Here an example closer to the engineering requirement for the model is presented.

This case is for a circular bore tunnel and examines the difference in vibration caused by the presence of a simple concrete lining. The analysis is presented here merely to provide an illustration of the use of the software, and does not represent a specific location.

The model for the unlined tunnel is shown in Figure 4. A single boundary element domain is used with a small finite element domain representing the solid concrete tunnel invert. In Figure 4, the boundary elements are shown each having a normal vector facing inwards towards the material represented by the domain. The three-noded boundary elements are 0.4 m long. The ground properties are taken as typical of a deep drift of clay being similar to those used

in [13] where a semi-infinite finite element model was used to study vibration propagation from a circular bore tunnel. The material parameters of the ground are an S-wave speed of 610 ms^{-1} and a P-wave speed of 1500 ms^{-1}; the density of the material has been assumed to be 1700 kgm^{-3} and the loss factor, 0.15. The surface of the ground is represented to distances +50 m and -20 m relative to the vertical centre-line of the tunnel.

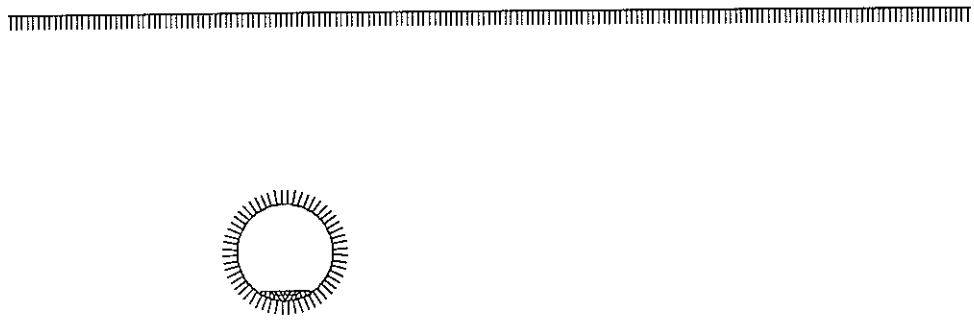

Figure 4. Model for the unlined tunnel.

The tunnel has a 7 m diameter and is situated at a depth of 20 m below the ground surface at the rail-head level. The response is calculated to a unit load (1 N) divided between the two rail positions on the tunnel invert. The loading positions are shown in Figure 5 which shows the FE mesh for the tunnel ring. The ring is 0.2 m thick and has material parameters representing concrete (Young's modulus, 37.6×10^{9} Nm^{-2}; Poisson's ratio, 0.15; density, 2400 kgm^{-3} and a loss factor of 0.03). The model for the lined tunnel has the same definition of the boundary element domain as for the unlined tunnel.

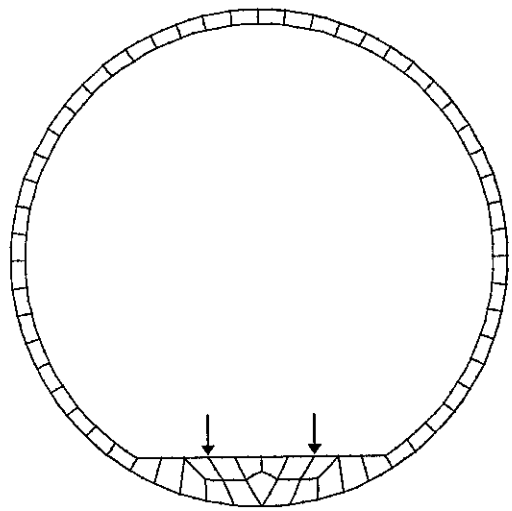

Figure 5. Close up of the tunnel part of the model for the lined tunnel case showing the loaded nodes corresponding to the positions of the rails.

The model produces the vertical and lateral degree of freedom responses as the complex amplitudes at each node of the model and at each frequency of the solution. A large amount of data is therefore produced and, in common with other numerical modelling methods, the data can be presented in different ways to examine the behaviour of the system.

5.2 Spatial distribution of response

Figures 6 and 7 show the displacement response amplitude at 100 Hz for the unlined and lined tunnels. Here the response is plotted from the point at $x = 0$ m (directly over the tunnel crown) to $x = 45$ m. It can be seen that the character of variation of vibration amplitude with distance is different in the two cases although at the larger distances the general levels of each of the lateral and vertical components are similar for the lined and unlined tunnels. In this region the vertical component dominates.

Both responses contain local dips in the response at certain distances. These are due to interference patterns in the wave field. It may be expected that these would not emerge so strongly were it not for the precise geometry of the boundaries and homogeneity of the material defined in the model. In practice the ground has ill-defined geometry at its boundaries and is randomly inhomogeneous. Measurements of vibration on the ground would therefore not show these localised features. In any case it would not be feasible to measure at many locations and it is usual for measurement results to be presented in terms of one-third octave band analysis which would tend to smooth out the variation observed in these single frequency results.

Over the tunnel, for distances less than about 20 m, the responses of the two tunnels are different in character from those at greater distances. The unlined tunnel has a maximum response at this frequency on the surface at about 20 m whereas the maximum response for the lined tunnel is closer to the tunnel centre-line. In the region over the tunnel crown, the levels of the lateral and vertical components are similar to one another.

For distances less than 20 m (the depth of the tunnel) the response is greater for the lined tunnel than for the unlined case at this frequency. For distances greater than this the reverse is true.

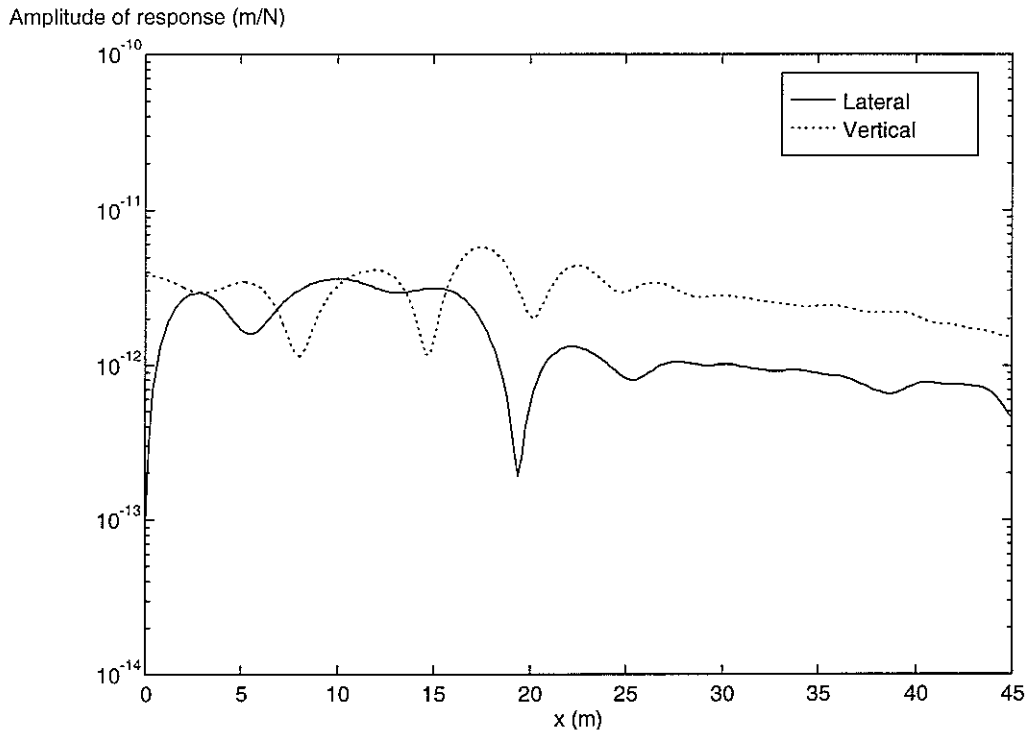

Figure 6. Response along ground surface at 100 Hz for the unlined tunnel.

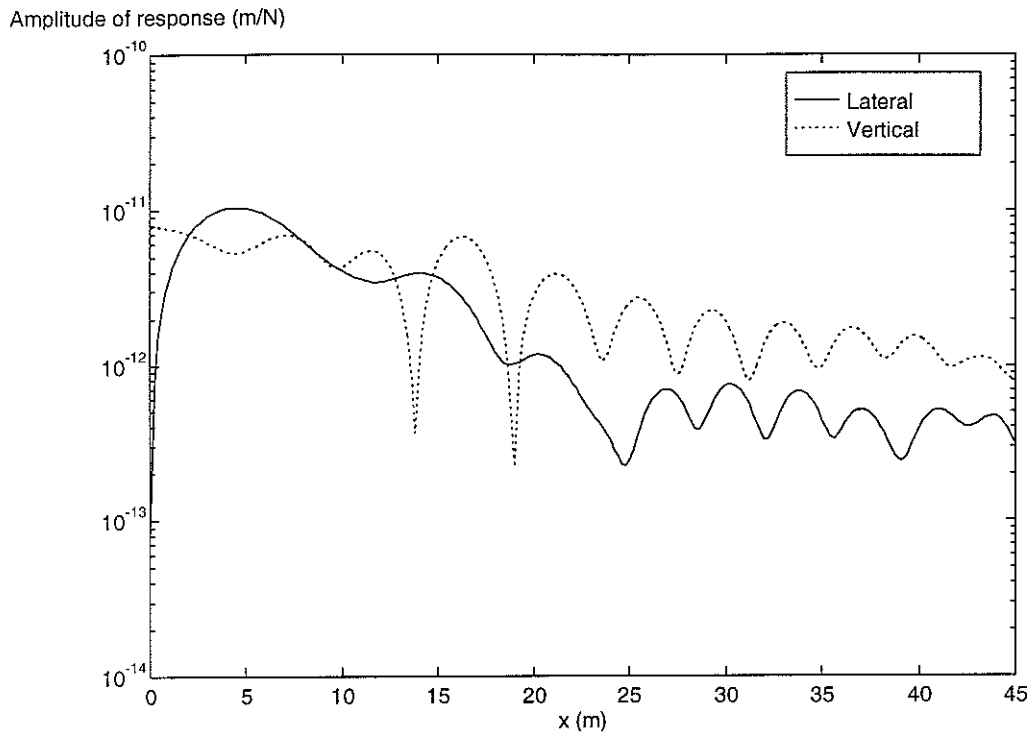

Figure 7. Response along ground surface at 100 Hz for the lined tunnel.

Figures 8 and 9 present the data in a different way, showing the displacement of the nodes at the tunnel at an instant of time (*i.e.*, phase in the harmonic cycle). Again the results are plotted for a single frequency of 100 Hz. These Figures show the response of the tunnel ring in the two cases. (An enhancement to this type of presentation can be achieved by animation of the results on a computer screen.) A comparison of Figure 8, for the unlined tunnel, with Figure 9 shows that a stronger response is carried to the crown (top) of the tunnel in the lined structure than in the unlined case. At this frequency, where the shear wavelength (about 6 m) is smaller than the diameter of the tunnel, the 'radiation' of vibration from the tunnel invert (base) is directional and, for the response directly above the tunnel, the tunnel invert is not as important a source as that represented by the crown. Indeed, for distances along the surface, to a point approximately equal to the depth of the tunnel, the tunnel itself shields the ground surface from the vibration at the invert. The lined tunnel, however, transmits vibration to the crown. This explains the transition in the character of the responses along the surface shown in Figures 6 and 7.

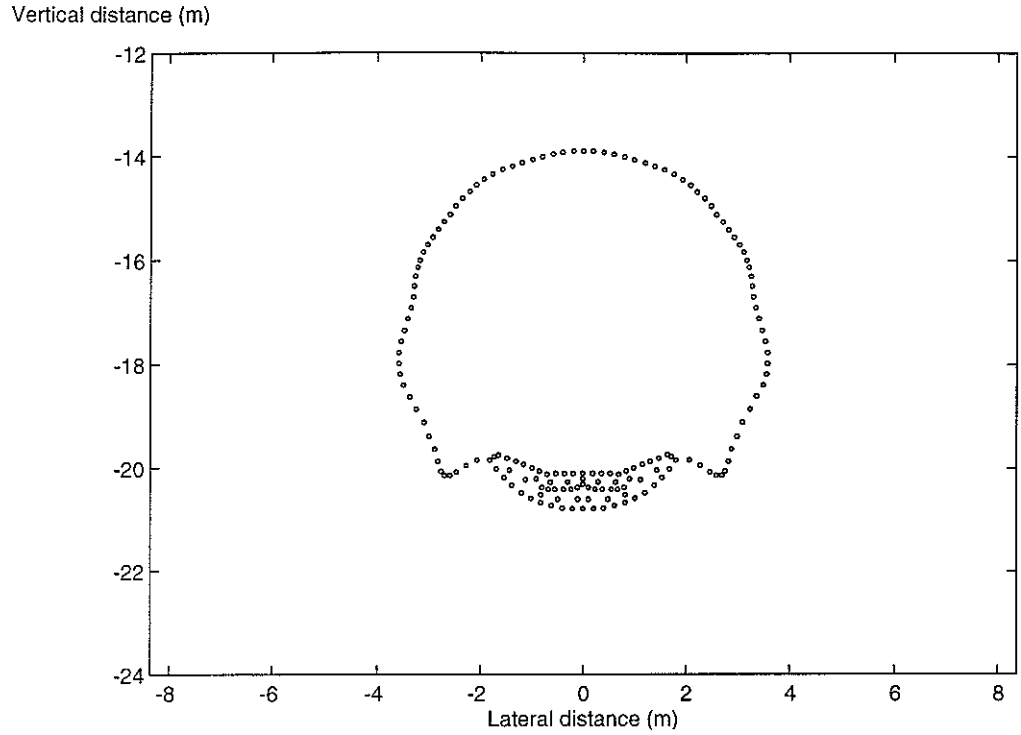

Figure 8. Response showing waves round tunnel ring at 100 Hz for the unlined tunnel ring.

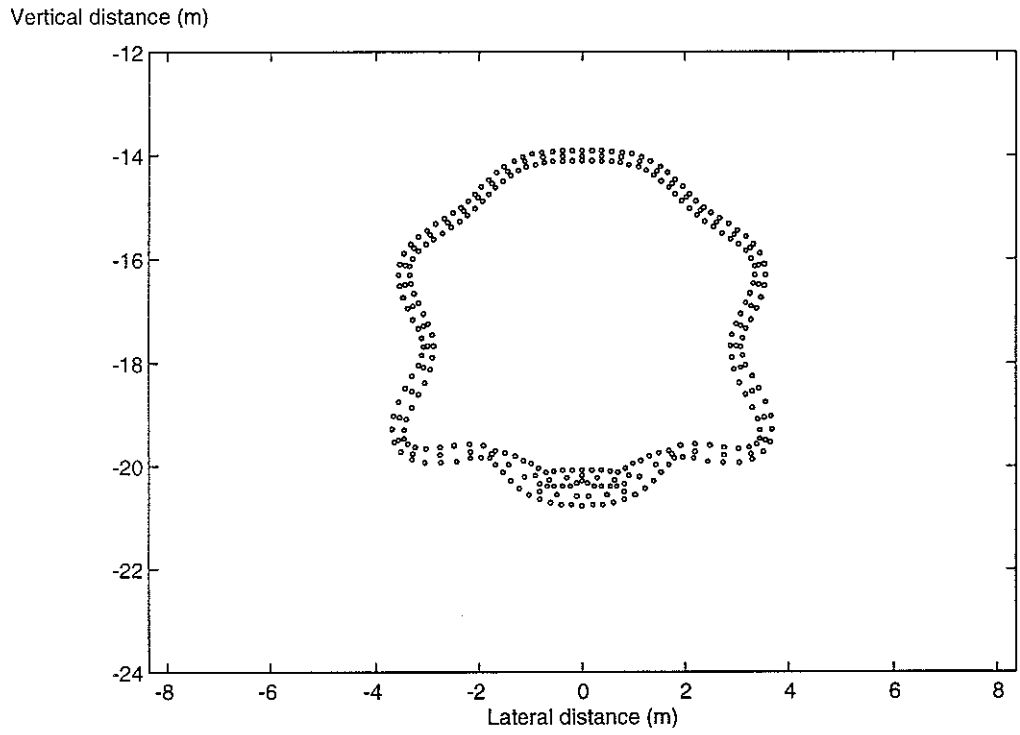

Figure 9. Response showing waves round tunnel ring at 100 Hz for the lined tunnel ring.

5.3 Frequency responses

Measured data is usually presented as frequency responses at particular locations. The vertical response at the tunnel invert, *i.e.* directly under one of the applied loads is shown for the unlined and lined tunnels in Figure 10 for 45 frequencies logarithmically spaced. It shows that at low frequencies the impedance of the lined tunnel is higher due to the stiffness of the structure

and the mass of soil that the tunnel structure carries with it. The tunnel lining becomes uncoupled from the invert for frequencies above approximately 30 Hz due to the onset of bending waves in the lining. The point responses above this frequency are very similar for the two tunnels. The small peak just above 100 Hz corresponds to an internal resonance of the tunnel invert. This can be seen to be a little more pronounced for the unlined tunnel, than for the case with the concrete lining.

Figures 11 and 12 show the frequency responses at the ground surface at points 20 m and 40 m from the tunnel centre line respectively for excitation at the invert as before. Figures 13 and 14 show the corresponding frequency responses for the lined tunnel. These frequency responses show a number of peaks and dips and it is difficult to compare the characteristics of the two tunnels on this basis by examining frequency responses at single points in the soil.

These frequency responses confirm that, as seen for the single frequency in Figures 6 and 7, the vertical response is the greater for most of the frequency range for these two locations. The vibrational response at a particular point on the surface of the ground is an elliptical particle motion. The orientation of the ellipse and therefore on the relationship between the vertical and lateral resolved amplitudes depends of the precise phase relationship of the waves propagated to that point in the ground. For real soils and structures there are a number of factors that randomise the phase relationships of waves propagated to a receiver point in the soil and the two components of response are unlikely to exhibit behaviour that is so distinct.

Here the data are examined at a precise point on the ground surface and it is not known, at a particular frequency, whether the response at the location chosen may be at a dip in the response in the variation of response spatially as seen at some frequencies in Figures 6 and 7.

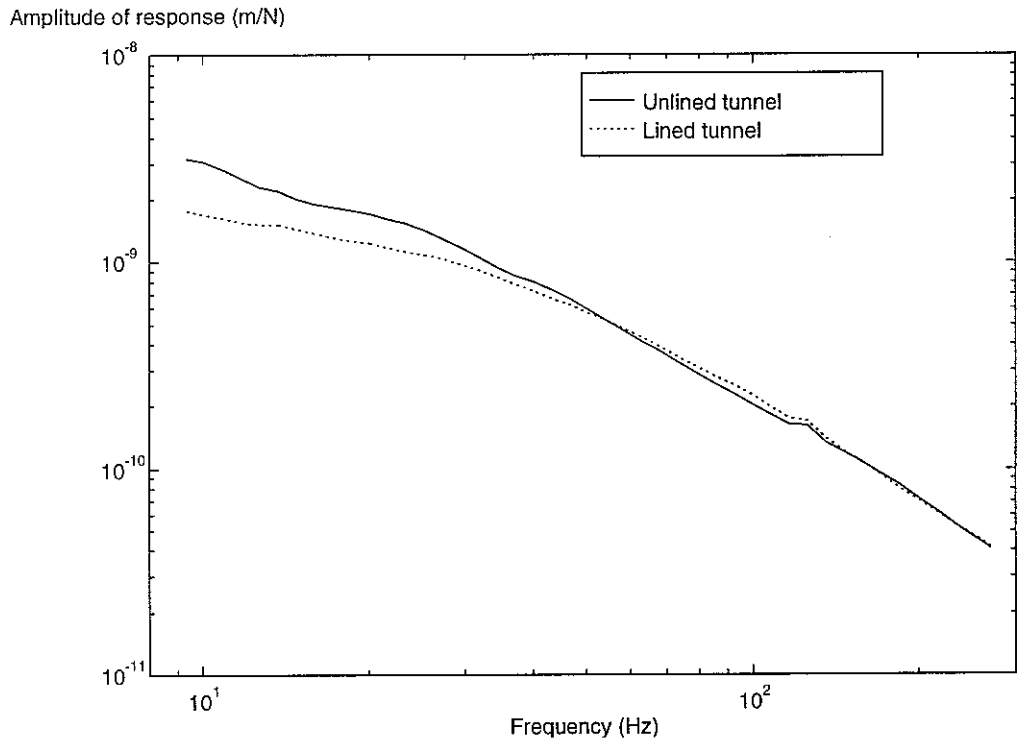

Figure 10. Response under one of the rail positions on invert for the lined and unlined tunnels.

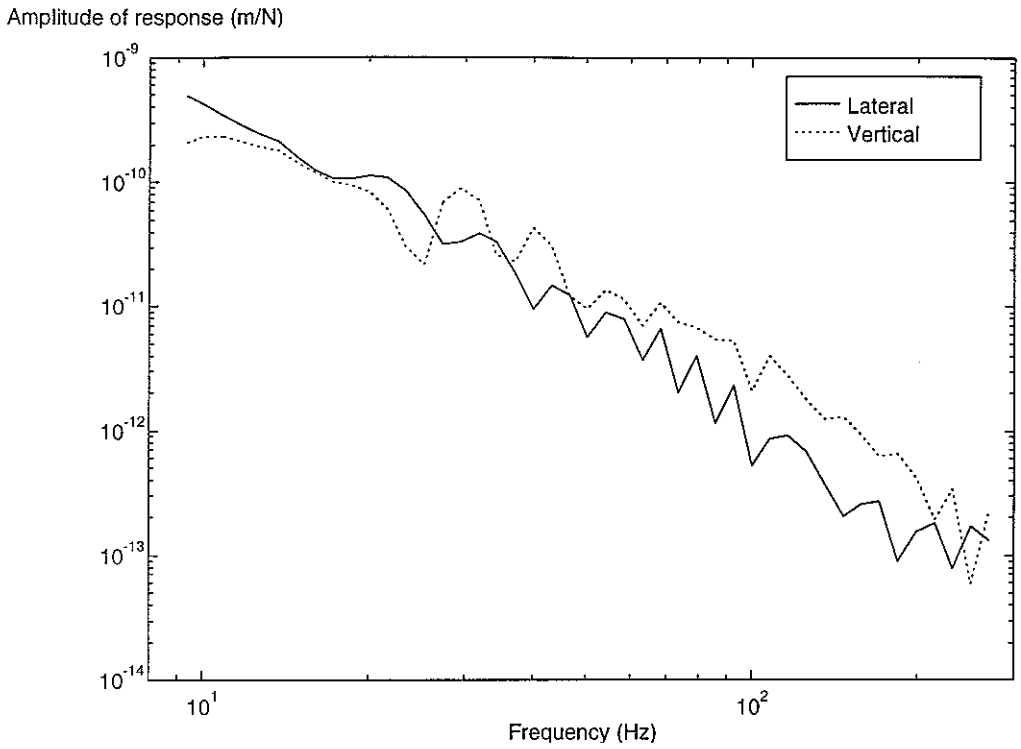

Figure 11. Frequency response from the unlined tunnel at the surface 20 m from the tunnel centre-line.

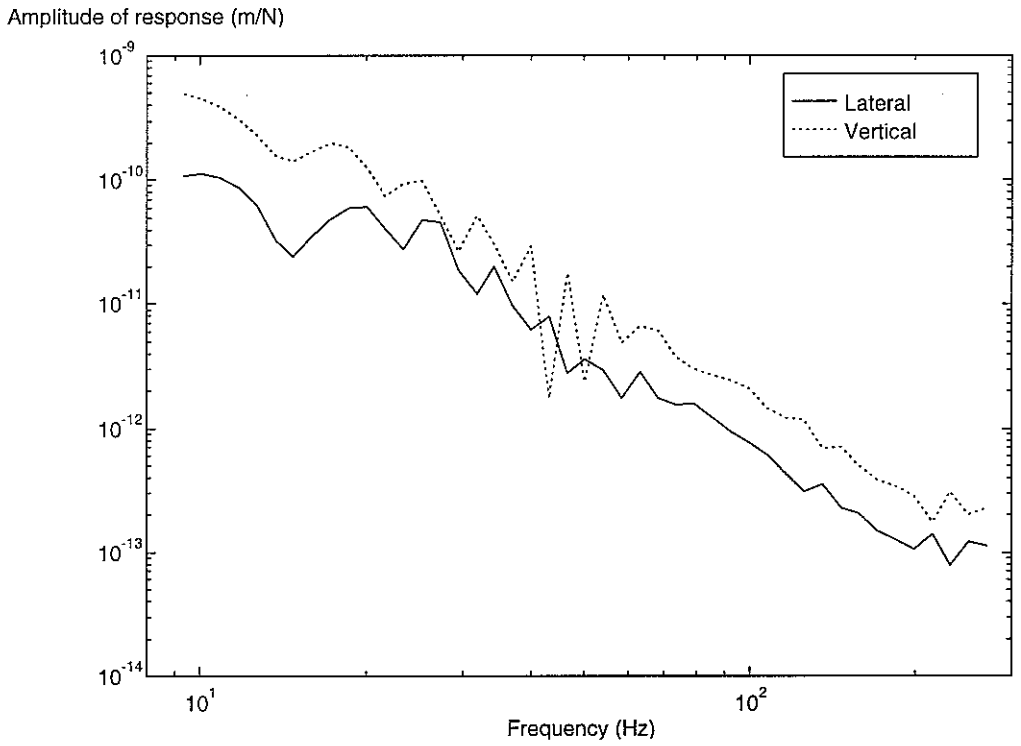

Figure 12. Frequency response from the unlined tunnel at the surface 40 m from the tunnel centre-line.

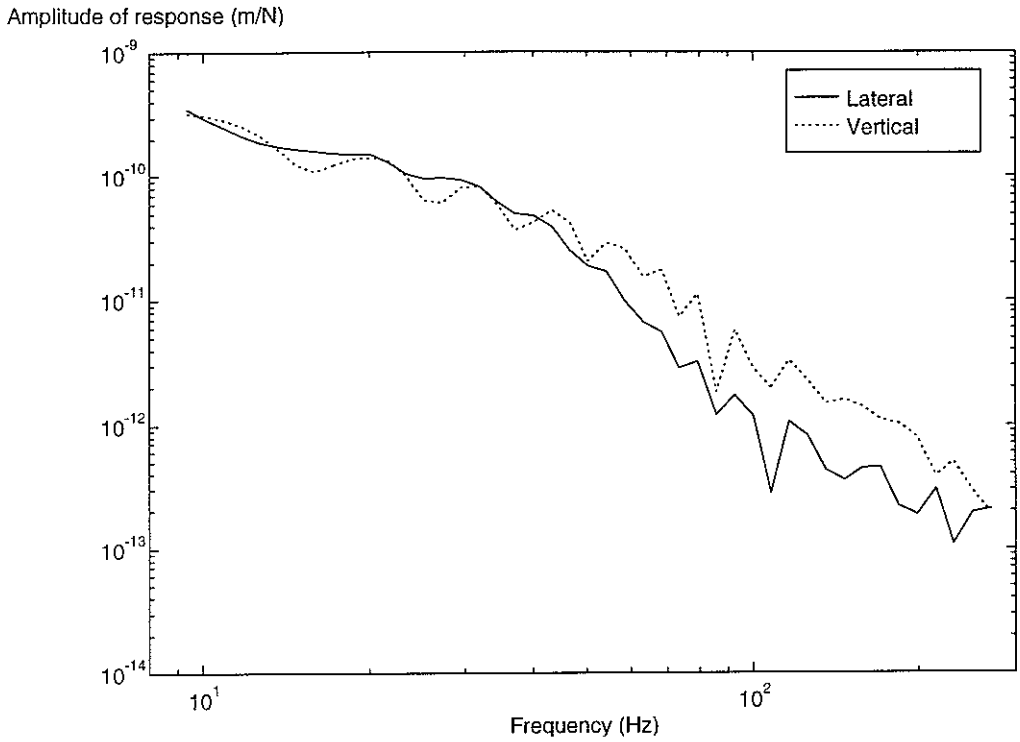

Figure 13. Frequency response from the lined tunnel on the surface 20 m from the tunnel centre-line.

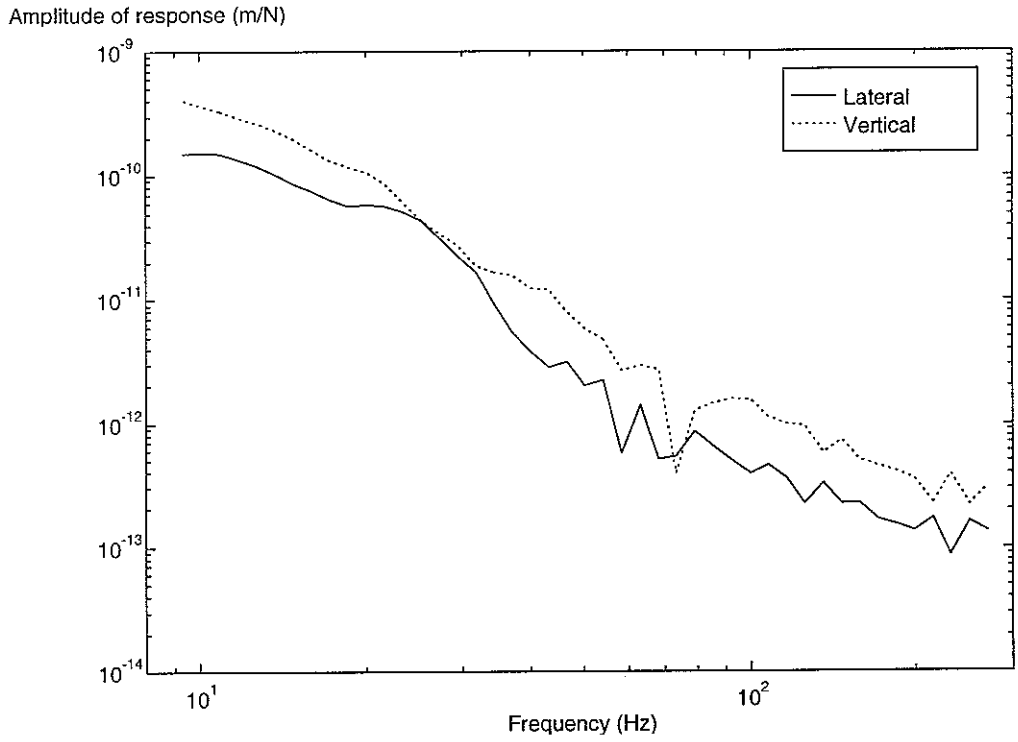

Figure 14. Frequency response from the lined tunnel on the surface 40 m from the tunnel centre-line.

5.4 Averaged responses

In this section the responses are presented in the form of averages in both spatial and frequency domains in order to show a more generalised comparison of the performance of the two tunnel structures. This is appropriate where the environmental vibration from the two structures is to be compared over a range of distance at the ground surface for a range of frequency.

In order to combine the vertical and lateral components to form a single measure of the amplitude, independent of its direction, the response has been evaluated as

$$u = \sqrt{|u_x|^2 + |u_y|^2}$$

This 'pseudo-resultant' has been used previously in [2] and [13] as a generalised measure of the response. The square of the pseudo-resultant has then been averaged in one-third octave frequency bands for each node. The deciBel level has then been averaged spatially using a running mean with a baseline of 5 m. The results of this process are presented for the 25 Hz, 50 Hz, 100 Hz and 200 Hz bands in Figure 15. In this figure the lined and unlined tunnel responses are plotted.

It is now more easily seen that the lined tunnel gives rise to higher levels of vibration above the tunnel. The shading effect of the tunnel for these locations can be seen most clearly in the 200 Hz band. At distances from about 20 m to 45 m the unlined tunnel gives rise to higher vibration in the 25 Hz, 50 Hz and 100 Hz bands but at 200 Hz the responses at 45 m are approximately equal.

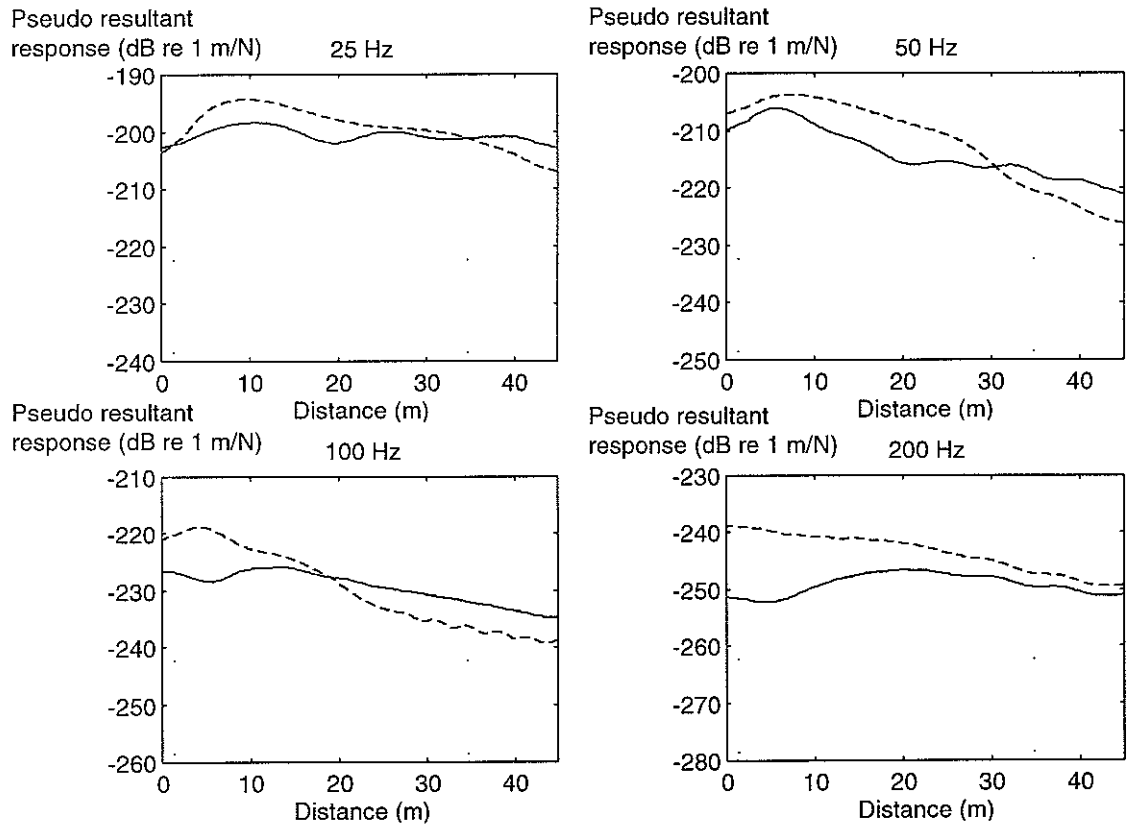

Figure 15. Comparison of response of lined and unlined tunnels after frequency averaging into one-third octave bands and spatial averaging over 5 m baseline (—— unlined; - - - - lined).

6. A CUT AND COVER TUNNEL

In order to provide a demonstration of the use of the model for a different type of structure cut-and-cover tunnel has been studied. This is plotted in Figure 16. Again this is for a notional case. The tunnel structure is 12.4 m wide and 7 m deep being large enough to accommodate a double track bed. The ground surface is modelled using boundary elements from -15 m to +50 m relative to the tunnel centre-line. The track base is not represented in the model. Rather, a unit amplitude force is distributed over a 3 m width of the ground under the location of the right-hand track. The abutment walls were attributed properties typical of masonry and are 2.2 m thick at their bases. The roof of the tunnel is attributed properties that correspond to a first bending resonance of around 16 Hz. This part of the structure is 1 m thick. The ground has an S-wave speed of 250 ms^{-1}, a P-wave speed of 1200 ms^{-1} and a density of 1900 kgm^{-3}. Table 1 gives the material properties of each of the materials in the model. The frequency response has been calculated at 51 frequencies covering the 5 Hz to 200 Hz one-third octave bands.

Figure 16. Mesh for the cut-and-cover tunnel model showing boundary element normals.

A modified model of the tunnel is shown in Figure 17. This incorporates foundation engineering under the abutment walls. This is implemented in the model as stiffened blocks of soil modelled using separate BE domains. The foundation engineering may be taken to represent an array of small-scale concrete piles or stiffened soil. The material parameters used for the stiffened soil are given in Table 1. An additional BE domain is also included under the centre of the tunnel for computational efficiency. This has the same properties as the unmodified soil.

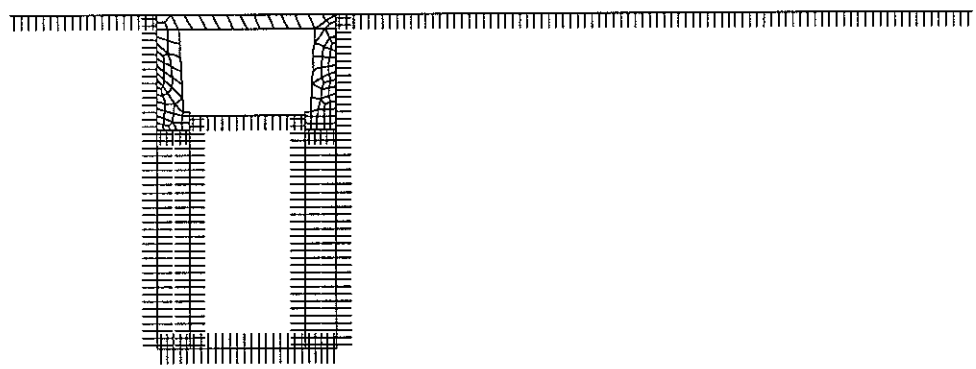

Figure 17. Mesh of tunnel with foundation engineering under abutment walls

Table 1 Material properties used in the cut-and-cover tunnel models

	Young's modulus ($\times 10^9$ Nm^{-2})	Poisson's ratio	Mass density (kgm^{-3})	Loss factor
Roof	16.4	0.3	2400	0.25
Walls (masonry)	11.2	0.15	2400	0.5
Soil	0.359	0.478	1930	0.1
Stiffened soil	1.64	0.47	1940	0.1

The behaviour of the structure is complicated and subject to high damping, the effect of radiation of energy away in the soil being greater than that of material damping. At about 16 Hz the roof of the tunnel has a first bending resonance with higher order resonances throughout the frequency range above this. Near 20 Hz the abutment walls bounce on the stiffness of the support of the ground. Effects of the coincidence of the wavelength in the soil with the overall width of the structure also occur near this frequency. Higher in the frequency range, many other interactions take place with the walls exhibiting bending behaviour and internal modes etc. Figure 18 shows the instantaneous displaced shape of the structure without stiffened soil at 37 Hz. At this frequency a rocking resonance of the walls on the soil stiffness can be discerned.

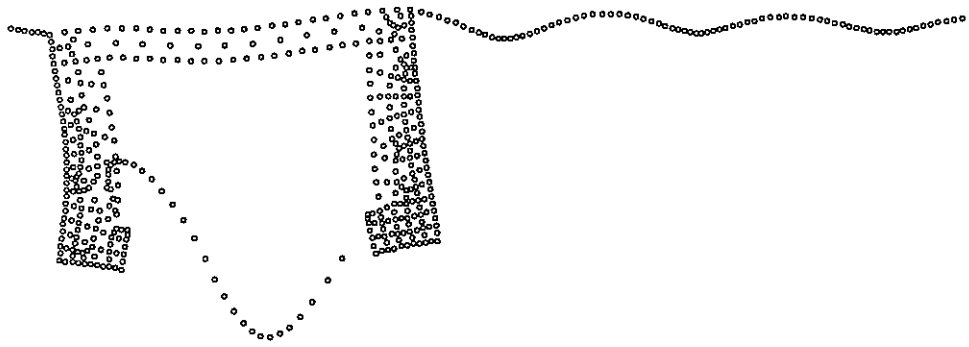

Figure 18. Displaced shape plot of part of the model at 37 Hz.

The frequency response under the centre of the load (direct receptance) is shown in Figure 19. The response under a 3 m wide load acting on a homogeneous half-space, calculated using an exact model, is also plotted on this graph. It can be seen that the results for the tunnel cases are close together and even at low frequency the effect of the foundation engineering on the at response directly under the track is not very great. Effects due to the mass of the tunnel structure, its dimensions (forming a cavity in the soil half-space), etc. cause the direct receptance of the ground in the presence of a tunnel structure differ from the half-space result. This is the case even at 5 Hz. Nevertheless, the general shape and level of the direct receptance spectrum still follow those for the homogeneous half-space. The dip that is common to all three results at about 150 Hz corresponds to a wavelength of the Rayleigh wave being about half the width of the track load. At this frequency some cancellation of the effect of the input occurs across the width of the vibration source.

The vertical response at the centre of the roof of the tunnel is shown in Figure 20. Broad peaks in the response can be seen near the bending resonances of the roof around 16 Hz, 40 Hz and 100 Hz. The peaks are sharper for the structure with strengthened foundations as the

vibration of the roof is less directly coupled to radiation of vibration into the soil at the abutment walls. At low frequency the strengthened structure has a lower response than the unstrengthened structure.

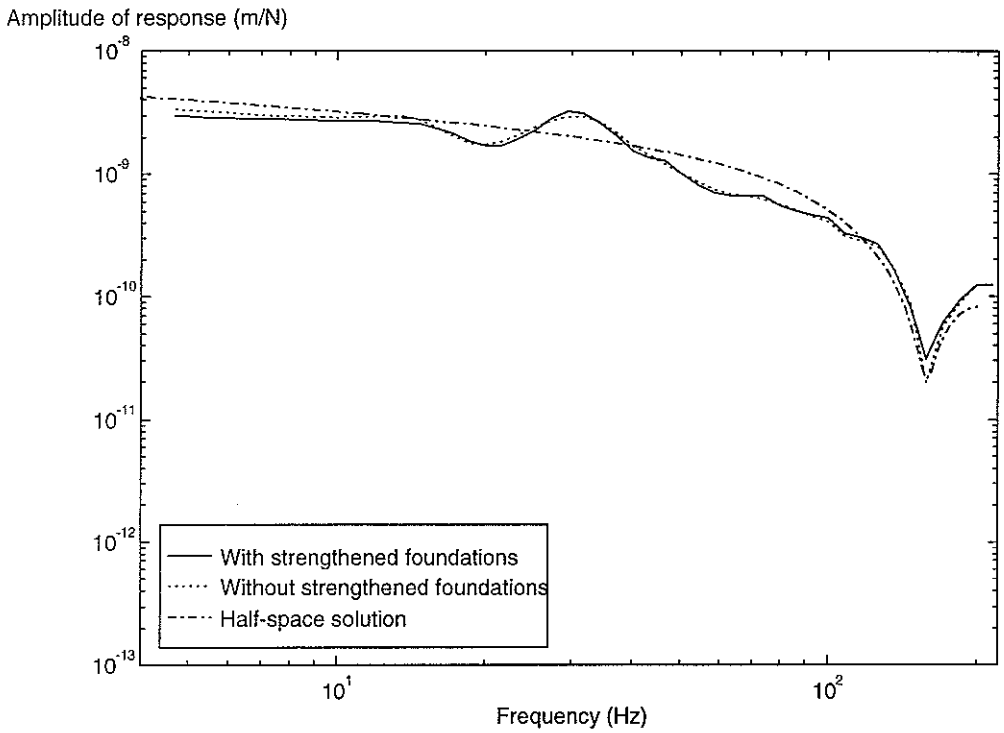

Figure 19. The frequency response of the ground under the centre of the load.

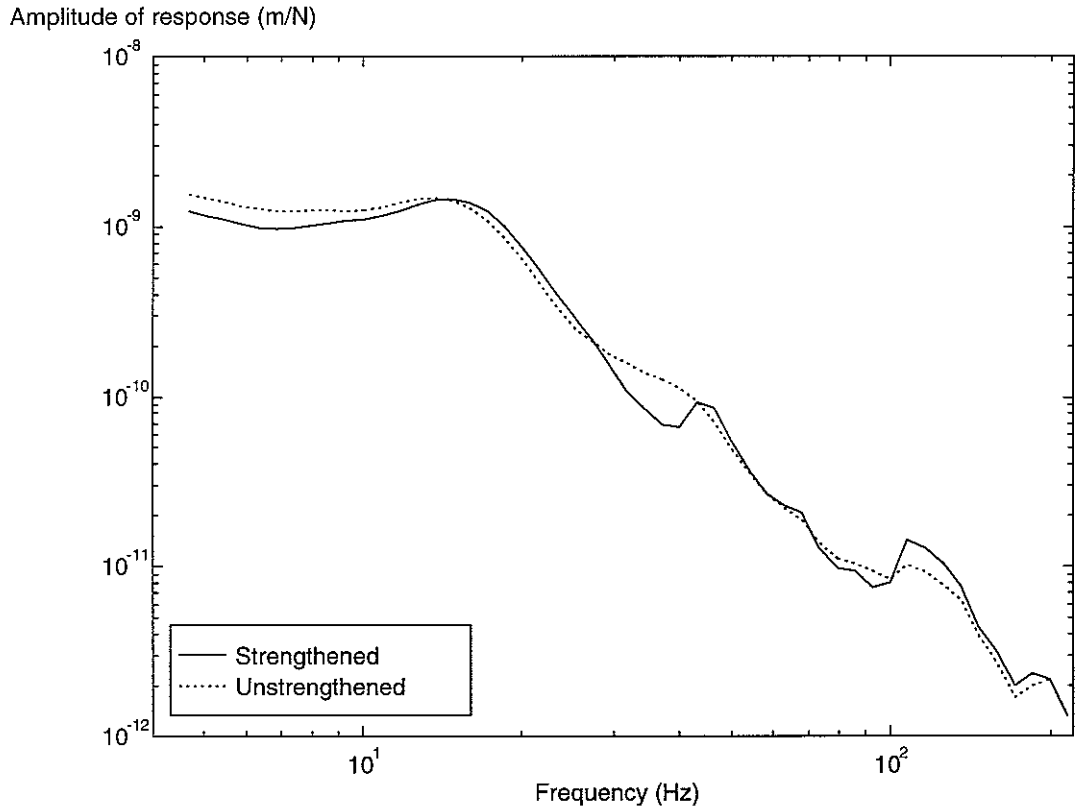

Figure 20. Vertical amplitude of response at the centre of the roof for the cut-and-cover tunnel with and without strengthened foundations.

The vertical and lateral responses of the ground surface 20 m from the centre-line of the tunnel are shown in Figure 21. At most frequencies the vertical response is greater than the lateral. From this response at a single position the effects of the foundation strengthening are difficult to assess in any overall way.

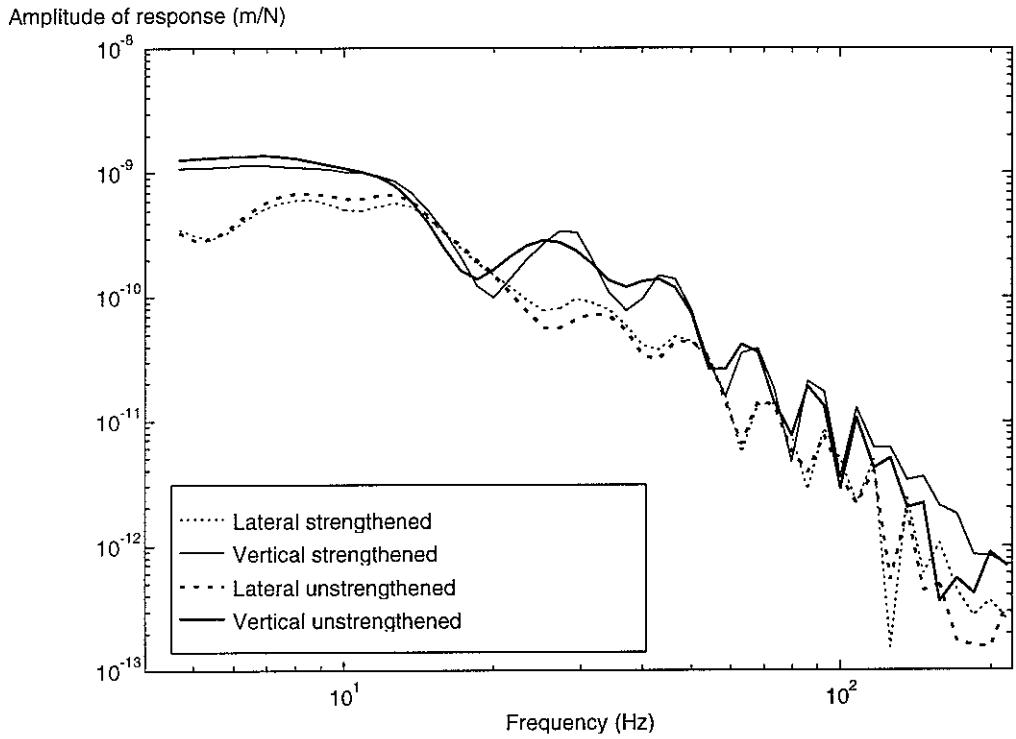

Figure 21. Vertical and lateral amplitudes of response on the ground surface at 20 m from the centre line of the cut and cover tunnel with and without strengthened foundations.

The effects of the foundation engineering on the vibration propagation from the tunnel given in the same frequency- and spatially-averaged terms as Figure 15 for the bored tunnel, are presented in Figure 22. Here results at lower frequencies are also shown than for the bored tunnel as the lower frequency, 'feelable' vibration is more likely to be of interest in this case.

It can be seen from Figure 22 that the highest levels of vibration are generally observed not on the roof of the tunnel but on the ground to the side of it. At low frequencies the rate of decay with distance is small compared to that at high frequencies.

Figure 22 shows that at low frequencies up to about 25 Hz the foundation engineering produces a small reduction in transmitted vibration levels. This is greatest for the lowest frequency band shown. This is in line with the substantial increase in static foundation stiffness that would be the primary objective of piling and may reduce whole-body perceptible vibration from heavy axle load trains significantly. However, at frequencies of relevance for structure-borne noise the increase in dynamic foundation stiffness is small. At the 50 Hz band and the 100 Hz band the vibration transmitted from the stiffened structure is slightly higher than the unstiffened structure and in highest frequency band, 200 Hz, for distances beyond 20 m an increase in response of up to about 8 dB is predicted. However, the vibration excited by a train at 200 Hz is likely to be very low and is strongly attenuated with the distance from the tunnel in this region. At 200 Hz waves propagating down the stiffened soil columns enhance the radiation to the field beyond the immediate influence of the abutment walls themselves, which have a lower response at this frequency in the stiffened case.

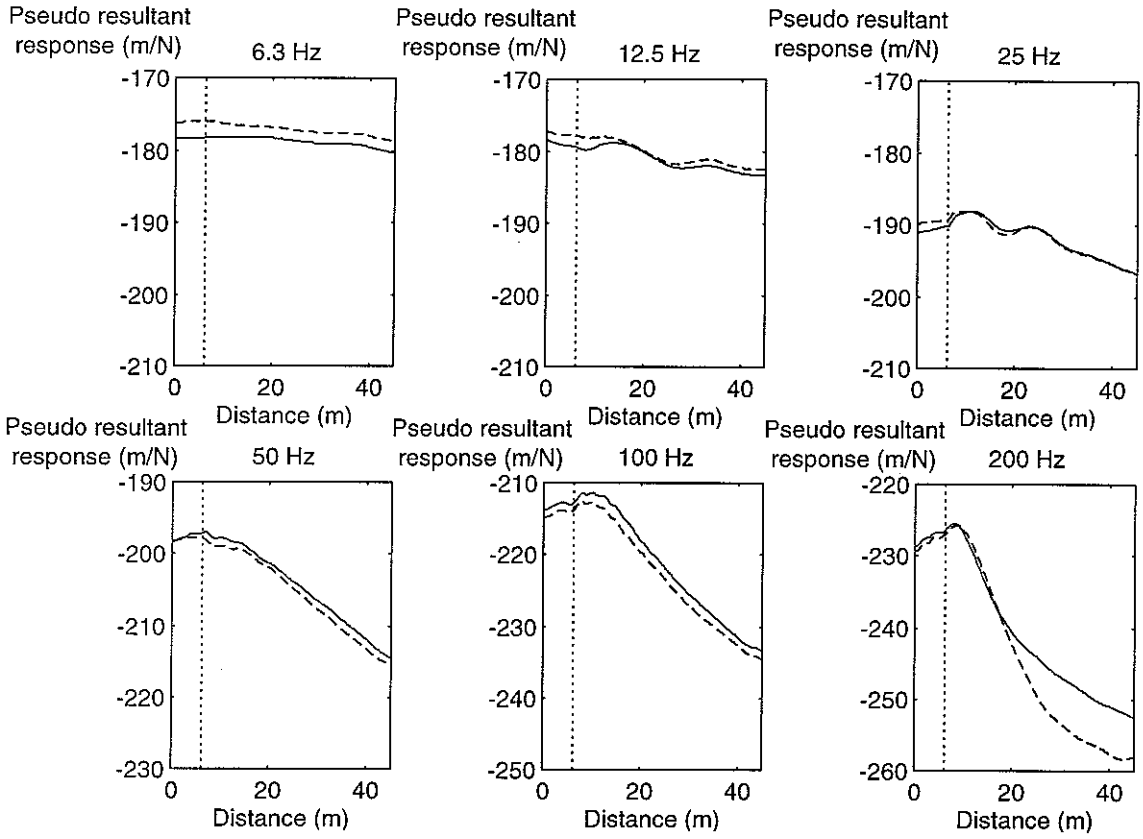

Figure 22. Comparison of surface response of cut-and-cover tunnels after frequency, and spatial, averaging (—— strengthened; - - - - unstrengthened, vertical line indicates edge of tunnel structure).

7. CONCLUSIONS

The theory of a coupled boundary element/finite element model for the propagation of vibration in a two-dimensional medium has been presented. This combines the ability of the boundary element method to model an infinite medium with the advantages of the finite element method to model inhomogeneous structures. A number of boundary element and finite element domains can be coupled together. A method for the analysis of the propagation of vibration through the ground that can encompass buried structures and ground layers of differing materials is therefore derived. The theory is implemented in a program that is described in a separate report in which the nature of the numerical error is also studied. The present report describes two example analyses: a bored tunnel with and without a lining and a cut-and-cover tunnel with and without foundation engineering. By this means it is demonstrated that the model can be used for the analysis of engineering situations covering the frequency range of interest to the study of ground-borne noise (up to about 200 Hz) within reasonable computing resources.

The results from the example cases are presented in different ways. Plots showing the displacement at a single frequency at an instant of time (or as an animation) can be used to gain an understanding of the behaviour of the structure. Graphs of the frequency response at single point locations and graphs of the variation of response amplitude with distance for single frequencies provide too complicated a picture for the study of environmental vibration. In order to overcome this difficulty a frequency-averaged, and spatially averaged 'pseudo-resultant' is proposed.

8. ACKNOWLEDGEMENT

The work reported has been carried out, and the program described in this report has been developed, under EPSRC grant number GR/L11397.

9. REFERENCES

1. Peplow, A.T., Jones, C.J.C. and Petyt, M 1995 *Proc. Inst. Acoustics*, 17(4), Liverpool, 479 - 486, Ground vibration over uniform and non-uniform layered media: a two-dimensional model.

2. Peplow, A.T., Jones, C.J.C. and Petyt, M 1999 *Applied Acoustics* 56, 283 - 296, Surface vibration propagation over a layered elastic half-space with an inclusion.

3. Von Estorff, O. and Kausel, E. 1989 *Earthquake Engineering and Structural Dynamics,* **18**, 1065 - 1075, Coupling of boundary and finite elements for soil-structure interaction problems.

4. Jones, C.J.C., 1994 *Proceedings of the Institution of Civil Engineers, Transportation* **105**, 43 - 51. Use of numerical models to determine the effectiveness of anti-vibration systems for railways.

5. Jones, C.J.C., 1996 *Proceedings of Internoise '96,* Liverpool, 421 - 426. Groundborne noise from new railway tunnels.

6. Jones, C.J.C., Thompson, D.J. 1999 *ISVR Technical Memorandum No. 838*, A boundary element model for two-dimensional elastodynamics on a single open or closed domain.

7. Jones, C.J.C., Thompson, D.J. and Petyt, M., 1999 *ISVR Technical Memorandum No. 840,* TEA - a suite of computer programs for elastodynamic analysis using coupled boundary and finite elements.

8. Dominguez, J. 1993 Computational Mechanics Publications, Southampton (Elsevier Applied Science.) Boundary elements in dynamics.

9. Mustoe, G.G.W. 1980 *PhD Thesis, Swansea University,* A combination of the finite element and boundary integral procedures.

10. Tullberg O. and Bolteus L. 1982 *Boundary Element Methods in Engineering, Ed. C.A. Brebbia,* Springer, Berlin, 625 - 635, A critical study of different boundary element stiffness matrices.

11. Petyt, M 1990 *Introduction to finite element vibration analysis*, Cambridge University Press.

12. Jones, D.V. and Petyt, M. 1993 *Journal of Sound and Vibration* **161**, 1-18. Ground vibration in the vicinity of a strip load: an elastic layer on half-space .

13. Jones, C.J.C., Wang, A. and Dawn, T.M. 1995 *Computational Acoustics and its Environmental Applications, Ed. C.A. Brebbia,* Computational Mechanics Publications, Southampton, 285 - 292, Modelling the propagation of vibration from railway tunnels.